3D Printed Scaffolds for Stabilization and Local Therapeutic Delivery in Bone Metastases

Audrey A. Pitaru

Department of Experimental Surgery, McGill University, Montreal

December, 2022

A thesis submitted to McGill University in partial fulfillment of the requirements of the degree of Master of Science (in Experimental Surgery)

Table of Contents

Abstract

Bone is the third most common site for cancer metastasis, with breast and prostate tumors often the primary source. The current gold standard of treatment involves surgically removing large sections of the affected bone. An important limitation is that small amounts of residual tumor are often left behind. With patients' survival time increasing, they are faced with high risk of recurrence and re-operation. 3D printing is garnering attention as a solution to overcome this limitation, as it is cost-effective and produces unique, patient-specific geometries. In this study, we aim 1) to generate composite implants from two polymer types, a stiff lactide-mineral material (Lactoprene) which supports bone repair, and a sponge-like polymer (Lay FOMM), which can be loaded with therapeutics for local delivery; 2) to test the scaffolds' mechanical integrity and ability to deliver chemotherapeutics to breast and prostate cancer cells *in vitro*. We hypothesize that composite scaffolds will have comparable mechanical strength to trabecular bone and composite scaffolds with chemotherapeutics will be equally effective at inhibiting tumor cell proliferation and migration *in vitro* compared to direct chemotherapeutic treatment. Compression testing was performed on Lactoprene, and Lactoprene-Lay FOMM composite scaffolds. The release of doxorubicin was quantified over a period of 1 week using a fluorescence microplate reader. Doxorubicin and cisplatin were loaded onto composite scaffolds which were then incubated with MDA-MB-231 breast cancer and C4-2B prostate cancer cell lines to determine metabolic activity via AlamarBlue assays. A mixed migration model (MMM) assay was conducted by combining a 3D cell culture model consisting of MDA-MB-231 cells treated with composite scaffolds loaded with doxorubicin to assess metabolic activity and cell migration. Lactoprene and composite

scaffolds exhibited similar compression properties. The relative IC_{50} was determined for doxorubicin and cisplatin, for both MDA-MB-231 and C4-2B cell lines. The composite scaffolds were loaded with varying amounts of doxorubicin and over 50% was released over 7 days for all groups. A significant reduction in metabolic activity was observed with MDA-MB-231 and C4-2B cells treated with composite scaffolds loaded with doxorubicin compared to control composite scaffolds loaded with PBS ($p < 0.0001$). There was no significant difference between composite scaffolds loaded with doxorubicin in MDA-MB-231 or C4-2B cells compared to direct doxorubicin treatment. MDA-MB-231 and C4-2B cells treated with composite scaffolds loaded with varying doses of cisplatin caused a significant reduction in metabolic activity compared to controls ($p < 0.0001$). Composite scaffolds were equally effective at inhibiting tumor cell migration compared to direct treatment in the MMM. There is currently an unmet need for enhanced reconstruction post-resection. 3D printed scaffolds are promising for the delivery of effective doses of chemotherapeutics to reduce the proliferation of cancer cells and prevent recurrence. Future research may assess the *in vivo* efficacy of these scaffolds in terms of bone repair and tumor recurrence.

Résumé

L'os est le troisième site le plus courant de métastases cancéreuses, les tumeurs du sein et de la prostate étant souvent la principale source. L'étalon-or actuel du traitement consiste à enlever chirurgicalement de grandes sections de l'os affecté. Une limitation importante est que certaines cellules tumorales restent cachées. La durée de survie des patients augmentant, ils sont confrontés à un risque élevé de récidive et de réintervention. L'impression en 3D attire l'attention en tant que solution pour surmonter cette limitation, car elle est rentable et produit des géométries uniques et spécifiques au patient. Dans cette étude, nous visons 1) à générer des implants composites à partir de deux types de polymères, un matériau lactide-minéral rigide (Lactoprène) qui favorise la réparation osseuse, et un polymère ressemblant à une éponge (Lay FOMM), qui peut être chargé de thérapeutiques pour leurs livraisons; 2) tester l'intégrité mécanique des échafaudages et leur capacité à administrer des agents chimiothérapeutiques aux cellules cancéreuses du sein et de la prostate *in vitro*. Nous émettons l'hypothèse que les échafaudages composites auront une résistance mécanique comparable à celle de l'os trabéculaire et que les échafaudages composites avec chimiothérapie seront tout aussi efficaces pour inhiber la prolifération et la migration des cellules tumorales *in vitro* par rapport au traitement chimiothérapeutique direct. Des tests de compression ont été effectués sur des échafaudages composites Lactoprene et Lactoprene-Lay FOMM. La libération de doxorubicine a été quantifiée sur une période de 1 semaine à l'aide d'un lecteur de microplaques à fluorescence. La doxorubicine et le cisplatine ont été chargés sur des échafaudages composites qui ont ensuite été incubés avec des lignées cellulaires de cancer du sein MDA-MB-231 et de cancer de la prostate C4-2B pour déterminer l'activité métabolique via les tests

AlamarBlue. Un test de modèle de migration mixte (MMM) a été réalisé en combinant un modèle de culture cellulaire en 3D composé de cellules MDA-MB-231 traitées avec des échafaudages composites chargés de doxorubicine pour évaluer l'activité métabolique et la migration cellulaire. Les échafaudages en lactoprène et en composite présentaient des propriétés de compression similaires. La IC_{50} relative a été déterminée pour la doxorubicine et le cisplatine, pour les lignées cellulaires MDA-MB-231 et C4-2B. Les échafaudages composites ont été chargés avec des quantités variables de doxorubicine et plus de 50 % ont été libérés sur 7 jours pour tous les groupes. Une réduction significative de l'activité métabolique a été observée avec les cellules MDA-MB-231 et C4-2B traitées avec des échafaudages composites chargés de doxorubicine par rapport aux échafaudages composites contrôles chargés de PBS ($p < 0,0001$). Il n'y avait pas de différence significative entre les échafaudages composites chargés de doxorubicine dans les cellules MDA-MB-231 ou C4-2B par rapport au traitement direct à la doxorubicine. Les cellules MDA-MB-231 et C4-2B traitées avec des échafaudages composites chargés avec des doses variables de cisplatine ont entraîné une réduction significative de l'activité métabolique par rapport aux contrôles ($p < 0,0001$). Les échafaudages composites étaient tout aussi efficaces pour inhiber la migration des cellules tumorales par rapport au traitement direct dans le MMM. Il existe actuellement un besoin non satisfait de reconstruction post-résection améliorée. Les échafaudages imprimés en 3D sont prometteurs pour l'administration de doses efficaces de produits chimiothérapeutiques afin de réduire la prolifération des cellules cancéreuses et de prévenir les récidives. Des recherches futures pourraient évaluer l'efficacité *in vivo* de ces échafaudages en termes de réparation osseuse et de récidive tumorale.

Acknowledgements

There are so many people that helped me in one way or another to get me to the point of being able to write these acknowledgements for my thesis. I am thankful for each part every one of you have played, big or small, mentioned or remembered.

I am enormously thankful for my supervisors, Dr. Derek Rosenzweig, and Dr. Isabelle Villemure. Derek, you guided me in innumerable ways and always pushed me to do more. I don't know what I would have done without your support. It is thanks to you that I was able to achieve all that I did in the last three years. Dr. Villemure, I am thankful for your biweekly meetings filled with direction, questions, and advice. You asked me to complete tasks ahead of schedule and it was always beneficial. That along with your words of encouragement kept me on track.

The feedback I received during my research advisor committee meetings was imperative. Thank you, Dr. Veena Sangwan, Dr. Rahul Gawri, Dr. Lisbet Haglund, and Dr. Michael Weber. The time and thought put in was evident and much appreciated. I also feel incredibly grateful and privileged to have had my research funded by CIHR.

Thank you Ateeque. There are not enough words to encompass my gratitude for having you as a lab partner and friend. You truly were there every step of the way for this master's. You answered every (silly) question, humored me with 12-hour surgery days, went on donut runs, read my drafts, played an immense part in my thesis, and even delivered bubble tea chats in between. I am forever grateful.

I am thankful for every single one of my lab members, but I would be remiss if I did not mention these wonderful people. I am thankful for Gabe who first trained me in 3D printing, wrote a paper with me, and tried to teach me the engineering aspect, even if I had very little background.

Thank you, Meg and Hyeree for training me when I had never previously stepped foot in tissue culture, for answering a million questions, for teaching me so I could do on my own, and for all your guidance. I am incredibly thankful for Mansoureh. You fit running an experiment with me into your busy schedule and you were always so kind and understanding.

It takes a lot of people to create a thesis, and some of them are behind the scenes. Troy, you have been an amazingly supportive partner throughout this arduous, yet fulfilling and invaluable journey. When I fell behind in life duties to fulfill lab ones, you took on the burden. When I felt I could not, you helped me pick myself back up and made sure I could. I cannot thank you enough for making sure everything else was okay so I could focus on my master's. I am grateful for my friends who were the most encouraging and caring people throughout, giving me the extra push when I needed it most. Finally, I will always be indebted to my mother, who does everything from the bottom of her heart, and has taught me to do the same. You have supported every decision I've made since I could walk and talk and have been there for me without fail, making the completion of this M.Sc. possible.

Contribution of Authors

This work consists of one manuscript ready for submission for publication. The contributions for the manuscript are the following:

Audrey Pitaru (candidate): Methodology, all experiments, formal analysis, writing original draft, reviewing and editing.

Ateeque Siddique: Experimental support, formal analysis, writing original draft, reviewing and editing.

Mansoureh Mohseni Garakani: MMM experiment, formal analysis, reviewing and editing.

Isabelle Villemure: Conceptualization, supervision, reviewing and editing.

Derek Rosenzweig: Conceptualization, supervision, reviewing and editing.

List of Tables

List of Figures

List of Abbreviations

β-TCP: β tricalcium phosphate

3D: three-dimensional

A1G7: 1% alginate-7% gelatin

CAD: Computer Aided Design

CT: computerized tomography

Dox: doxorubicin

FBS: fetal bovine serum

FDM: fused deposition modelling

GFP: green fluorescent protein

hMSC: human mesenchymal stem cells

MMM: mixed migration model

MRI: magnetic resonance imaging

PCL: polycaprolactone

PEG: polyethylene glycol

PET-CT: positron-emission tomography-CT

PFA: paraformaldehyde

PLA: polylactic acid

PLLA: poly-L-lactic acid

PMMA: polymethylmethacrylate

PP-3D-S: plasma-modified, electro-spun, nanofibrous 3D scaffold

PVA: Polyvinyl alcohol

RFP: red fluorescent protein

STL: stereolithography

X-rays: radiographs

Chapter I: Rationale and Objectives

There has been a recent increase in cancer incidence, as well as advancement in treatment, resulting in increased patient longevity. This in turn gives rise to an increase in the risk of metastatic cancer. Bone is the third most common site for metastases, with breast, prostate, and lung tumors often cited as the primary source [1]. Bone metastases can cause pain, biomechanical instability, and pathological fractures [2]. The spine is the most common site of bone metastases. The current gold standard of treatment for large lesions in the bone is surgical resection. Although bone can heal on its own, the surgical excision often results in a defect that is too large to spontaneously heal. Furthermore, following resection, patients undergo systemic radiation therapy to remove residual tumor resulting in many side effects [3]. Due to the increased survival time, recurrence and re-operation are even more prevalent now. Another technique involves the reconstruction of the bone with acrylic cement. However, there are eventual reduced mechanical properties, and cement does not have anti-tumor effects [4]. Bone grafts are also used but are associated with donor-site morbidities and limited bone availability [5]. There is a need for a novel bone substitute material. An ideal method to overcome the current limitations is 3D printing as it is inexpensive and produces patient-specific geometries, allowing for patient-specific implants [6]. The overall goal for this research is to generate cost-effective 3D printed composite scaffolds with the capacity to locally delivery anti-cancer therapeutics following tumor resection. We have previously determined that local delivery of anti-tumor drugs inhibits osteolysis in a mouse tibia xenograft model [7]. The current study aimed to generate composite scaffolds from two polymer types, a stiff lactide material, Lactoprene, which supports bone repair, and a sponge-like polymer,

Lay FOMM 60, which can be loaded with therapeutics for local delivery. Another aim of the present study was to test the composite scaffolds' mechanical integrity and ability to deliver chemotherapeutics to cancer cells.

Chapter II: Literature Review

Spinal metastases

The term metastasis refers to the spread of cancer cells from their primary site where the tumor originated, to a secondary site where the cells settle and form a new tumor. The formation of the secondary tumor is referred to as the metastatic tumor, metastasis, or a secondary tumor [8]. Metastases to the spine are 20 times more frequent than primary spinal neoplasms and occur mostly in individuals between the ages of 40 and 70, as this age group is associated with an increased cancer risk [9], [10]. Spinal metastases are known to occur in 30-50% of cancer patients and the incidence and prevalence is expected to rise. These lesions significantly affect the quality of life of patients suffering from them, causing debilitating pain, neurological dysfunction, and paralysis [10]. Bone metastases can not only cause pain, but also biomechanical instability and pathological fractures [11]. Vertebral fractures and spinal cord injury severely erodes patients' quality of life. Over 10% of patients with spinal metastases have symptoms, the most common being pain in 90% of cases, and motor dysfunction being second in 35-75% of cases [8], [10], [12]. Cadaveric studies demonstrate that up to 90% of patients may have spinal metastases by the time of death [12]. These metastases predominantly occur in the thoracic vertebrae (70% of cases), followed by the lumbar spine (20%), cervical spine, and sacrum, and originate primarily from breast, prostate, lung, kidney, and gastrointestinal cancers [12], [13]. More specifically, spine metastases mainly arise initially in the posterior portion of vertebral bodies and the involvement of the pedicles follow suit [8]. Dissemination to the spinal cord (intradural) is rare [13]. The diagnosis of spinal metastases begins with pain as the initial symptom in 90-95% of patients; it is local and associated with

tenderness upon palpation of the spinous processes. All new onset neck or back pain in cancer patients is considered to be caused by spinal metastases until proven otherwise [14]. Interestingly, spinal metastases are the first manifestation of cancer in 12-20% of patients with associated symptoms. At the time of diagnosis, 38% to 76% of patients have neurological impairments (weakness, sensory and motor dysfunction) with half of them being unable to walk [14].

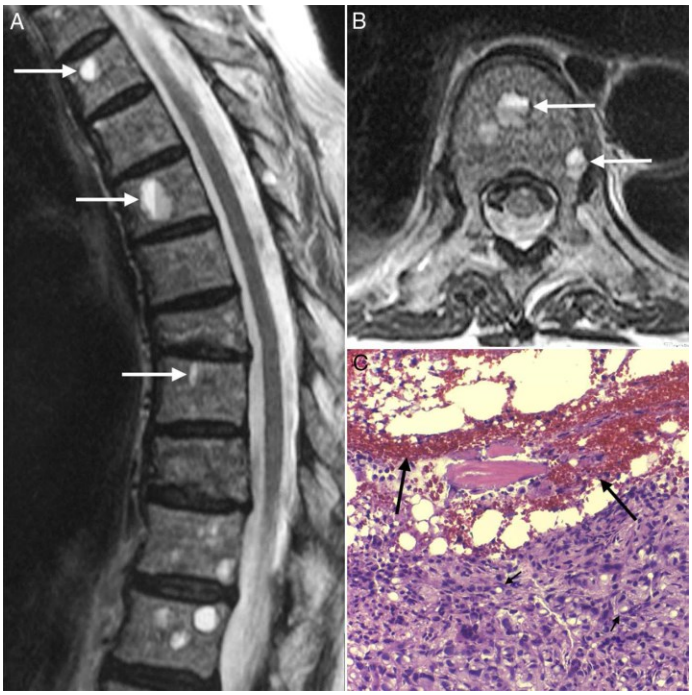

Figure 1-T. Spine magnetic resonance image showing a (a) sagittal and (b) axial projection of vertebral metastases. (c) Bone biopsy showing hematoxylin-eosin stain showing a poorly differentiated adenocarcinoma. Adapted from [15].

Diagnosis begins with laboratory studies and diagnostic imaging which may involve radiographs (X-rays), myelography, computerized tomography (CT), magnetic resonance imaging (MRI; Figure 1-T), bone scanning, and positron-emission tomography-CT (PET-CT) [14], [16], [17]. Proper treatment planning takes into consideration the clinical manifestations of the metastases (pain, neurological deficits), spinal stability, number of spinal metastases, the expected

degree of mobility the patient can attain, radiosensitivity and chemosensitivity of the tumors, and the patient's prognosis for survival [16]. Therapy goals are to control pain and preserve function, and multiple medical and surgical options for treatment exist and are provided to patients with spinal metastases.

Current treatments

Recent advancements in radiotherapy, oncology and surgery are resulting in increased longevity in patients with bone and spine metastases [1]. Following a complete neurological and oncological assessment with algorithms such as the NOMS decision framework (**n**eurological, **o**ncological, **m**echanical, and **s**ystemic), patients are provided with a dynamic treatment that involves recent advances in interventional radiology, radiation, medical oncology, and surgical techniques to optimize their outcomes [18]. Medical therapy involves systemic therapies such as chemotherapy (monotherapy or combination), hormonal therapy for breast and prostate cancer metastases, bisphosphonates to prevent bone resorption, radioisotopes to act as local radiation therapy, corticosteroids to reduce spinal cord edema, and analgesics for pain relief [10], [12], [16], [19]. In addition to side effects, chemotherapy plays a limited role in the treatment of spinal metastases [12]. Conventional external beam radiotherapy entails exposure of the entire vertebra to radiation, as well as one level above and below, thereby limiting the dose of radiation which can be given safely. Stereotactic radiosurgery, or stereotactic body radiotherapy, on the other hand, delivers high doses of radiation to a small target and may cause vertebral compression fractures [20]. However, a complication with all radiotherapy is the low tolerance of the spinal cord to radiation, often resulting in radiation myelopathy/myelitis after 9-15 months [19].

Surgery is often a first line of treatment for most cancers, including bone metastases, yet hidden cancer cells remaining in the tissue margins may lead to recurrence [21]. The excision of tumors is often extensive (*en bloc*) to ensure maximal excision and to decompress all neural elements, especially in patients with a better prognosis [10]. Furthermore, patients may undergo radiation therapy post-resection to eliminate residual tumor cells. However, the spinal cord has a lower radiation tolerance compared to the rest of the body, and some tumors are radioresistant [22], [23]. As tumors are vascularized, issues arise in surgery with extensive blood loss and pre-operative embolization to reduce bleeding may not always be an option due to anatomical variation. Minimally invasive surgery for patients with co-morbidities is an option thanks to advances in percutaneous instrument placement and visualization systems. Vertebral augmentation procedures (vertebroplasty or kyphoplasty) are minimally invasive techniques for stabilization and pain relief that are associated with low complication rates [10]. For more extensive resection, various implants exist for post-resection reconstruction of the affected vertebrae. Acrylic cement is commonly used for stabilization but has no regenerative potential or anti-tumor effects [24]. Bone grafting has potential for bone repair but is associated with donor-site morbidity and is limited in quantity [25]. The reconstruction of the anterior and middle columns of the spine may be achieved with acrylic cement secured with Steinman pins or a chest tube, titanium mesh cages, or expandable titanium cages, however, the issue of higher complication rates remain [12]. 3D printed scaffolds for spinal stabilization and local drug delivery are gaining attention to not only provide a biocompatible material for bone repair, but to locally deliver therapeutics and bypass the negative side effects associated with systemic drug administration.

3D printed scaffolds

Additive manufacturing, also called three-dimensional (3D) printing, is a relatively new fabrication process where 3D constructs are built layer-by-layer using 3D models. The long-standing manufacturing process has been subtractive in nature – starting with a block of material and taking away excess parts. Additive manufacturing is used in a myriad of industries and has countless applications, partly thanks to its open-source concept and ability to produce geometries and complex parts that prove too difficult for long-standing manufacturing processes that rely on a subtractive process. This has gained traction with tissue engineering as 3D printing can allow for additional control of the appearance and more precisely create the internal structures of scaffolds [4]. The medical industry in particular has seen a surge in additive manufacturing, specifically with regards to scaffold production [26]. Scaffolds are devices that can be implanted in patients and provide structural support and allow for tissue development [27]. Additive manufacturing allows for sophisticated, porous scaffold production, which is not possible with traditional manufacturing processes. 3D printing of scaffolds using polymeric materials can act as prototypes for tissue formation and regeneration [28]. Using the material extrusion printing technique, also called fused deposition modelling (FDM), many printing parameters can be controlled (Figure 2-T). This customizable approach allows for the components in the building of scaffolds to be optimized. Scaffolds made from FDM require less material and are therefore sustainable. They are also economical and can present good mechanical properties [29], [30].

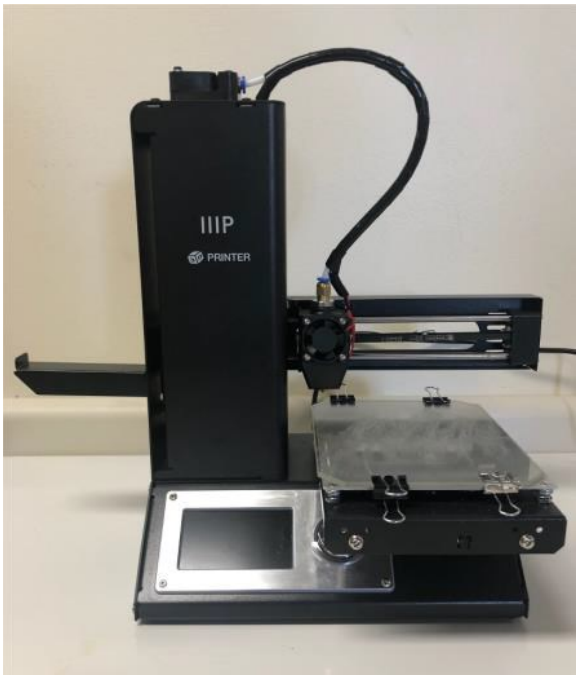

Figure 2-T. Image of Monoprice MP Select Mini v2 Fused Deposition Modeling Printer in the Rosenzweig Lab.

With 3D printing, a range of different biocompatible materials can be used to create scaffolds, including polymers, ceramics, metals, and hydrogels. This paper focuses on polymers, which are commonly used. Biodegradable thermoplastic materials have been widely studied for 3D printing bone substitutes, yet they possess limitations as a singular material. The use of thermoplastic polymer on its own lacks functionality and strength. Development of composite polymers has therefore allowed for better mechanical properties and functionality that cannot be accomplished by single materials. A solution has been to selectively mix composite polymers allowing for better mechanical properties and functionality that cannot be accomplished by the use of one material alone. This is done through mixing polymers with particle, fiber, or nanomaterial reinforcements [31].

Lay FOMM 60 and Lactoprene materials

Lay FOMM 60 is a flexible thermoplastic polyurethane copolymer that has a polyvinyl alcohol component that can be washed out. Once washed, Lay FOMM becomes a highly porous, sponge-like material. Lay FOMM has been used as a material in 3D printed scaffold design and is suitable for *in vivo* use and drug uptake and release in numerous studies. In one study, Lay FOMM was investigated as a device for drug delivery. It was used to release the chemotherapeutic doxorubicin, whereby 60-75% of the drug was released over 7 days [32]. Seeing as Lay FOMM is a novel material, not many studies have utilized it for tissue engineering purposes thus far. More specifically, its biodegradability has not been explored to our knowledge. Lactoprene is a medical-grade, strong, bioresorbable polymer manufactured and sold by Poly-Med, Inc. It is made up of 100% lactide and it is similar to polylactic acid, which is a commonly used filament in 3D printing. Lactoprene's biodegradability is an important factor for consideration in regard to implantation. A recent study determined the degradation profile of Lactoprene 7415 as a scaffold material for use in tissue engineering. It was found that Lactoprene exhibited excellent properties, whereby the degradation was quick enough that the remodeling process of bone cells was not disturbed, yet not too quick so there was sufficient mechanical stability [33]. Lactoprene is also sold as a composite mixed with β tricalcium phosphate (β-TCP), which has osteoinductive and osteoconductive properties. Work in our lab showed that Lactoprene mixed with β-TCP promotes bone formation *in vivo* and induces osteoconductive differentiation in a rat femur cortical window defect [34].

Breast and prostate cells

As breast and prostate cancer are often cited as the primary source for bone metastases, they were chosen as a model for bone metastases. The two cell types used in this study were MDA-MB-231 breast cancer cells and C4-2B prostate cancer cells. MDA-MB-231 is an epithelial, human

triple negative breast cancer cell line [35]. It is a highly aggressive, invasive, and poorly differentiated cell line that is commonly used in cancer research [36], [37]. C4-2B cells are prostate cancer cells that were derived from bone metastasis that grew in nude mice. Castrated nude mice were originally inoculated with LNCaP human prostate cancer cells, wherein the C4-2 cell line was derived. Subsequently, the C4-2 cells were injected in the bone of nude mice and the C4-2B cells were derived from this bone metastasis. C4-2B cells are often used as a preclinical model for metastatic prostate cancer [38].

Doxorubicin and cisplatin chemotherapeutics

Chemotherapeutics are agents that are used to treat cancers. These chemical compounds specifically target fast growing cells, which makes them ideal for cancer treatment since cancer cells grow more rapidly than most other cells in the body. Chemotherapeutics originate from natural sources or are the resultant of synthetic processes [39]. The two chemotherapy drugs explored in this study are doxorubicin and cisplatin, as they are both chemotherapy drugs commonly used to treat bone cancer [40]. Doxorubicin, derived from bacteria, is a standard chemotherapeutic used for treatment of many solid tumors in adult and pediatric patients. It is used to treat breast and prostate cancer, as well as bone sarcomas [41]. Doxorubicin is an anthracycline antibiotic that forms complexes with DNA, inhibiting DNA and RNA synthesis, as well as topoisomerase II activity, leading to DNA damage and apoptosis. Doxorubicin is generally slowly administered intravenously to patients [41], [42]. Cisplatin is another chemotherapeutic that is a platinum compound used for treatment of hematologic and solid tumor malignancies in both adult and pediatric populations [43]. This agent is used for numerous cancer treatments, including breast, prostate, and bone cancer [40], [44]. Cisplatin is an alkylating agent that causes platinum to bind to the purine bases in DNA [43]. It forms DNA adducts which prevents the repair of DNA and

subsequently induces apoptosis in cells [44]. The preferred method of administration for cisplatin is intravenously, but it can be administered intra-arterially [43]. Doxorubicin and cisplatin are administered intravenously or intra-arterially, which poses issues and results in numerous side effects. This type of treatment is a systemic chemotherapy. The most common, general side effects of chemotherapy are nausea, vomiting, hair loss, loss of appetite, mouth sores and diarrhea [40]. A specific side effect of doxorubicin is its association with acute cardiac toxicity [41]. Cisplatin has been associated with nephrotoxicity, cardiotoxicity and hepatotoxicity [45]. Local chemotherapeutic delivery overcomes a great deal of the limitations that exist with systemic chemotherapy. Some benefits of local delivery involve reduced side effects, including general chemotherapy side effects and toxicities to specific drugs, and targeted delivery whereby the drug does not need to circulate in the bloodstream before reaching the desired location. In addition, it could potentially avoid organ damage by leaving healthy tissue unharmed, allow for high concentrations of drug, reduce the need for postoperative chemotherapy and radiotherapy, and reduce the number of administrations of the drug [46].

Current implantable devices for bone repair and drug delivery

Indeed, the recurrence of tumors post-resection remains a significant challenge, and the administration of systemic chemotherapy compromises the quality of life of patients due to the associated negative side effects [47]. To overcome these challenges, implantable devices with controlled drug delivery capability for post-surgical cancer treatment are becoming increasingly important. Controlled drug delivery can also solve challenges associated with implants, such as pain, bacterial infections, poor osseointegration, immune rejection, and difficulty in personalizing treatment [48]. Implants may be made of metals, polymers, or ceramics, and serve to repair or replace the diseased bone that was removed [49].

Chen *et al*. coated titanium alloy bone implants with β-cyclodextrin to function as molecular reservoirs grafted onto chitosan molecules for the loading of calcitriol [50]. This coating allowed for the local release of calcitriol and promoted enhanced bone remodeling under osteoporotic conditions in a rabbit model, compared to the control titanium implants [50]. This is an example of how currently available implants are being modified to deliver drugs to improve the local effects. Titanium wires with titania nanotube arrays have also been investigated for drug-eluting purposes. Gulati *et al*. generated titanium Kirschner wires (bone fixation wires that pass through the skin) with an outer array of titania nanotubes for the delivery of the antibiotic gentamicin [51]. They determined that the drug release occurred in a two-phase manner with an initial burst release followed by a period with slower zero-order release kinetics [51]. Ultimately, implants with antibiotic-eluting features may be used for preventing infection. Polymers have also been examined for drug-release capabilities in orthopedic applications. Le Ray *et al*. encapsulated the antibiotic vancomycin into biodegradable poly(ε-caprolactone) (PCL) microparticles and determined that various preparation methods affected the release rates, ranging from 3% to 59% of the loaded drug released in 7 days [52]. They also showed that the drug-loaded microparticles did not significantly affect the viability of mouse fibroblasts [52]. This early study looked at the possibility of exploring polymers for drug delivery applications. Bose *et al.* explored polymers for the delivery of curcumin, an antioxidant and anti-inflammatory molecule that enhances osteoblast activity [53]. They used PCL, polyethylene glycol (PEG), and poly(lactic-co glycolic acid) together as a polymeric system acting as the reservoir to contain curcumin. They coated 3D printed β-TCP scaffolds with the drug-polymer solution and determined that different polymer combinations can affect the curcumin release rate differently, with the PCL/PEG combination showing the highest release [53]. They confirmed that the *in vivo* presence of the curcumin-loaded

scaffolds increased bone mineralization from 29.6% to 44.9% when compared to pure TCP scaffolds [53]. 3D printed scaffolds are gaining attention in the orthopedic drug-delivery field due to the flexibility of choice with regards to materials as well as the customizable and complex shapes that can be generated. Wu *et al*. prepared 3D printed calcium phosphate cement scaffolds for the local delivery of 5-fluorouracil, an anti-cancer drug, for bone cancer by developing a hydrophilic drug-loaded coating solution for the scaffolds using Soluplus, a pharmaceutical excipient, and PEG [54]. Their *in vitro* dissolution study showed a rapid drug release, with 100% of the drug released within 2 hours for all scaffolds [54]. As demonstrated by these studies, various drug coating and loading methods can affect the drug release kinetics. Multifaceted techniques can also be used to develop drug delivery devices. Zhang *et al*. combined the principles of PCL 3D printing, magnetic hyperthermia, and bioactive glass to generate a composite scaffold containing drug-loaded mesoporous bioactive glass particles [55]. They obtained a rapid release *in vitro* (~30%) on the first day followed by a relatively slow release for up to 10 days. Furthermore, these scaffolds contained Fe_3O_4 nanoparticles which provided them with a heating ability when exposed to a magnetic field. The scaffolds were able to experience a temperature change from 20ºC to 43ºC within 2 minutes [55]. 3D printing composite scaffolds allows for an integrated complex multi-purpose system revolving around local treatment for bone repair and drug delivery. Wang *et al*. implanted 3D printed poly-L-lactic acid (PLLA) scaffolds loaded with multiple chemotherapeutics into rats [56]. They demonstrated the high biocompatibility of PLLA scaffolds in rats which killed remaining cancer cells after a tumor resection with a high local dose [56]. The high local release of chemotherapeutics as demonstrated by this study have the capability to bypass the significant negative side effects associated with the systemic administration of chemotherapeutics.

As bone cement, which is a polymer, is typically used to reconstruct bones following a resection surgery, there is interest in developing cements loaded with chemotherapeutic drugs. Polymethylmethacrylate (PMMA) bone cement is commonly used in vertebroplasty applications and has shown encouraging results for chemotherapeutic delivery [57]. However, PMMA presents with several drawbacks as cements are not bioactive, do not allow for osseointegration, and the polymerization temperature can reach above 80ºC, causing tissue necrosis [58], [59]. Calcium phosphate cements are biocompatible and can promote bone regeneration; however, they are brittle and pose a challenge for load-bearing applications such as in the case of the spine [60], [61]. Hence, development of high strength composite 3D printed scaffolds for bone repair and drug delivery provides a great opportunity to overcome limitations with traditional implants. 3D printed constructs can be used for drug delivery applications and can be loaded with additives to stimulate osteogenesis [62]–[64]. With various materials to choose from, this technology allows for the customization of geometry, porosity, and layer-by-layer connectivity [64]. Research on the local delivery of antineoplastic drugs in orthopedic applications is limited, with most of the work to date conducted on antibiotics for the prevention of infection. 3D printing offers the field of orthopedic oncology a dynamic solution to incorporate biomaterials for the stabilization of bone, while delivering chemotherapeutics locally for treating the tumor and/or preventing recurrence, stimulating bone formation, and ultimately improving patient quality of life.

Chapter III: Manuscript

3D Printed Scaffolds for Stabilization and Local Therapeutic Delivery in Bone Metastases

Audrey A. Pitaru[1], Ateeque Siddique[1], Mansoureh Mohseni Garakani[1,2], Michael Weber[1], Lisbet Haglund[1], Abdellah Ajji[2], Michael Wertheimer[2], Isabelle Villemure[2], Derek H. Rosenzweig[1]

[1]Division of Orthopedic Surgery, Department of Experimental Surgery, McGill University, Montreal, Canada; [2]Department of Mechanical Engineering, Polytechnique, Montreal, Canada

Address correspondence and reprint requests to:

Derek H. Rosenzweig

Montreal General Hospital, C10.148.6

1650 Cedar Avenue, Montreal, Quebec, H3G 1A4

Tel: +1 (514) 934-1934 (ext. 43238)

Email: derek.rosenzweig@mcgill.ca

3D Printed Scaffolds for Stabilization and Local Therapeutic Delivery in Bone Metastases

Abstract

INTRODUCTION: The gold standard of treatment for bone metastases is surgical resection. The defect created by resection can be filled with 3D printed scaffolds with patient-specific geometries. We aim to generate composite implants from stiff (Lactoprene) and sponge-like (Lay FOMM) polymers loaded with chemotherapeutics for local delivery to prevent tumor recurrence, and to characterize their mechanical integrity. We anticipate these scaffolds will deliver effective doxorubicin and cisplatin chemotherapy to inhibit breast (MDA-MB-231) and prostate (C4-2B) cancer cell growth.

METHODS: Compression testing was performed on Lactoprene, and Lactoprene-Lay FOMM composite scaffolds. The release of doxorubicin was quantified over a period of 1 week using a fluorescent microplate reader. Doxorubicin and cisplatin were loaded onto scaffolds and were incubated with monolayer cultures of MDA-MB-231 and C4-2B cell lines to determine metabolic activity via AlamarBlue assays. Using a 3D model (mixed migration model), the metabolic activity and migration of MDA-MB-231 cells was assessed with the treatment of composite scaffolds loaded with doxorubicin.

RESULTS: Lactoprene and composite scaffolds behaved similarly in terms of compression testing properties. The relative IC50 was determined for all drugs and cell lines. The composite scaffolds were loaded with varying amounts of doxorubicin and over 50% was released over 7 days in all conditions. A significant reduction in metabolic activity was found with MDA-MB-231 and C4-2B cells treated with scaffolds loaded with doxorubicin or cisplatin compared to

control scaffolds ($p < 0.0001$). Composite scaffolds were equally effective at inhibiting tumor cell migration compared to direct treatment in the MMM.

CONCLUSIONS: There is currently an unmet need for enhanced approaches in surgical bone resection. These concerns can be addressed by developing mechanically stable 3D printed scaffolds that can deliver chemotherapeutics to reduce the proliferation of cancer cells *in vitro*. We show that the composite scaffolds are mechanically stable and are capable of releasing effective doses of chemotherapeutics for local delivery applications.

Introduction

Cancer metastasis remains a major challenge in oncology, often being the root cause of death, with metastasis accounting for 90% of cancer deaths [1]. Bone is the third most common site for cancer metastases, with breast, prostate, and lung tumors as the primary source [2]. Bone metastases are the most common cause of cancer-related pain, and these metastases often occur in the spine. Surgical intervention is often required for spinal instability and spinal cord decompression, and the resulting defect is often large with poor healing. In one study, 32% of patients with solitary spinal metastases developed locoregional recurrence after resection [3]. Since patient survival time is increasing with improved treatments, the risk of recurrence and re-operation is becoming more important. There is therefore a need for multifunctional bone substitutes to stabilize defects, promote bone repair, and block cancer recurrence.

Among the currently available bone substitutes, 3D printing has emerged as a cost-effective method to produce unique geometries allowing for patient-specific implants [4]. As for orthopedic applications, 3D printed scaffolds guide bone repair, can be fabricated using different materials and can locally deliver drugs [5]. A range of different biocompatible polymeric materials can be used to 3D print scaffolds, such as polymers, ceramics, and hydrogels. Biodegradable thermoplastic materials have been widely studied for 3D printing bone substitutes, yet they possess limitations as a singular material. The development of composite polymers has therefore allowed for better mechanical properties and functionality that cannot be accomplished by single materials. Poro Lay materials, such as Lay FOMM, are highly porous materials composed of a flexible thermoplastic polyurethane copolymer and polyvinyl alcohol (PVA). The PVA component is water-soluble, leaving a flexible, nanoporous, sponge-like structure suitable for *in vivo* use and drug uptake and delivery [7]. Lactoprene is a commercial, 100% lactide medical-grade material

similar to polylactic acid, a common filament used in 3D printing. Lactoprene is also available as a composite with β-TCP, which can be used in clinical applications, and we have shown it to be suitable for *in vivo* repair [8].

In this study, we set out to develop a composite scaffold from two polymer types, a Lactoprene shell incorporating a Lay FOMM core, with the aim of supporting bone repair and locally delivering a high dose of chemotherapy. The Lactoprene provides a mechanically strong lactide-mineral material directing bone repair, and the sponge-like Lay FOMM core is loaded with therapeutics for local delivery. We tested scaffolds' mechanical integrity to ensure that it has a comparable mechanical strength to trabecular bone, the chemotherapeutic release profile *in vitro* and the efficacy against breast and prostate cancer cell growth and viability. We hypothesized that 3D printed composite scaffolds will have comparable mechanical strength to trabecular bone and that the composite scaffolds with chemotherapeutics will be equally effective at inhibiting tumor cell proliferation and migration *in vitro* compared to direct chemotherapeutic treatment.

Materials and Methods

3D Printing

The 3D printing process was carried out on the Monoprice MP Select Mini v2 (Monoprice, Inc; Brea, CA, USA). The designing of the scaffold was done using SOLIDWORKS 2015 (Dassault Systèmes, SolidWorks Corporation, Waltham, MA, USA), a Computer Aided Design (CAD) software. The height and diameter of the scaffold was set to 2 mm and 3 mm, respectively. The hole in the center of the scaffold was set to 2 mm and the holes on the sides of the scaffolds were set to 0.5 mm. A representative image of the scaffold design is shown in Figure 1a. The CAD file was saved as a stereolithography (STL) file, which was sliced using Ultimaker Cura 4.3.0 (Ultimaker B.V.; Utrecht, Netherlands) software to attain the G code. The G code could then be used on the 3D printer with the selected filament to print the scaffolds layer by layer. All printing was performed indoors in a temperature-controlled environment. The printed scaffold is cylindrical-shaped with an empty center. A different porous filament is meant to be placed in the center of the scaffold to allow for drug uptake and release. The filament used for 3D printing was Lactoprene-100M (Polymed Inc). The printing parameters consisted of a 0.3 mm nozzle set to a temperature of 190°C, a bed temperature of 65°C, a printing speed of 20 mm/s, and the infill was set to 100%. The layer height was set to 0.175 mm, the flow rate was 100%, the retraction was enabled, and the printing speed was offset between 20% and 50% depending on the appearance of the scaffold during printing. A raft, which is a horizontal structure on which 3D printed parts are printed on top of, was used to ensure build plate adhesion. Thirty scaffolds were printed at a time on a raft. The filament used in the preparation of the scaffold was Lay FOMM 60 (MatterHackers; Burbank, CA, USA), which is a highly porous material.

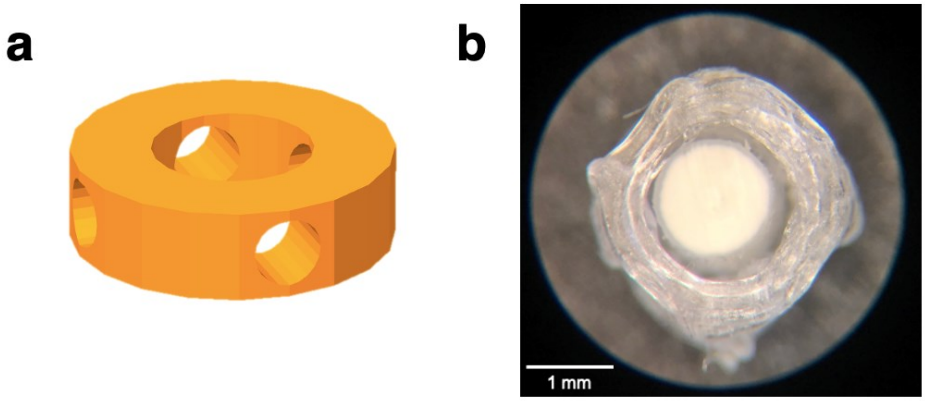

Figure 1. Scaffold visualization. (a) 3D CAD model design of outer scaffold shell. (b) Stereomicroscopy image of 3D printed scaffold made of Lactoprene shell with Lay FOMM 60 core insertion, viewed from top of scaffold. Scale bar = 1 mm.

Once the scaffolds were printed, they were removed from the raft surface. A 3D printed jig measuring tool was made with a 1 mm indent to ensure the pieces of filament to be placed inside the center of the Lactoprene scaffold were uniform. The Lay FOMM 60 filament was placed in the 1 mm indented portion of the 3D printed measuring tool and a razor blade was used to precisely cut off a 1 mm piece of the filament. This small piece of filament was then positioned inside the center of the 3D printed Lactoprene scaffold using tweezers. The composite scaffold was placed inside a plastic 15 mL centrifuge tube filled with double distilled water to wash out most of the rigid PVA. The water was changed every day in the morning and evening around the same time. After 3 days, the scaffolds were removed and placed inside another centrifuge tube with ethanol for 15 minutes for sterilization. Afterwards, the residual ethanol was allowed to dry off from the scaffolds at room temperature in a biological safety cabinet to maintain sterility. For additional sterilization, the scaffolds were left under UV lighting for 15 minutes and then turned over for an

additional 15 minutes. The scaffolds were stored in a sterile environment for subsequent steps. The washing and sterilization of composite scaffolds can be visualized in Figure 2b.

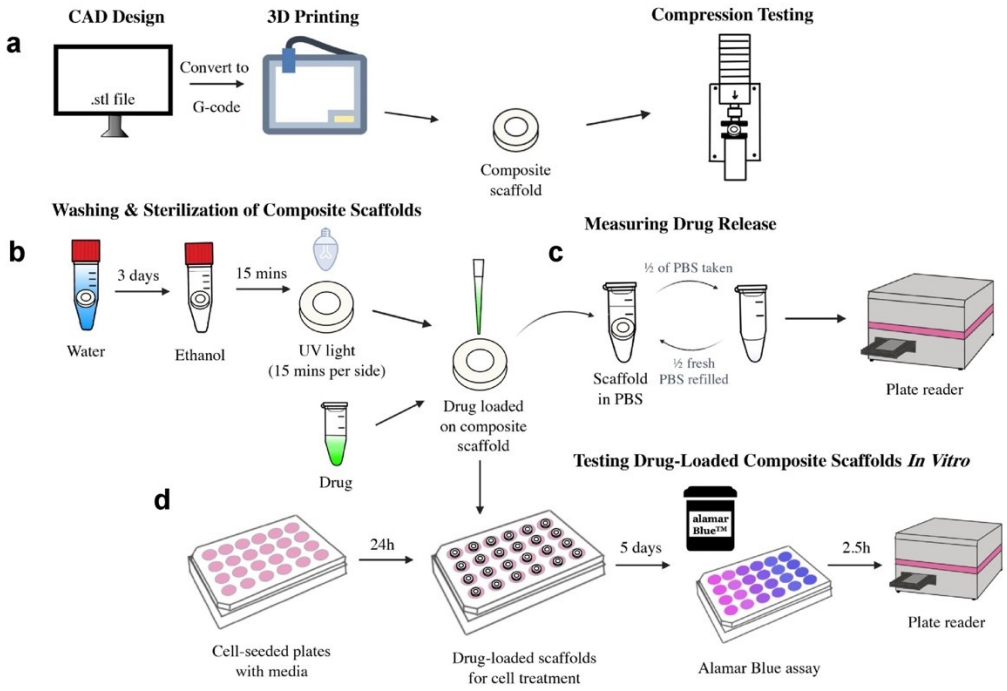

Figure 2. A schematic illustration of (a) the 3D printing of scaffold process from CAD design to printed scaffold, followed by compression testing; (b) washing and sterilization of 3D printed composite scaffolds; (c) drug release from 3D printed composite scaffolds by measuring fluorescence using a plate reader; (d) *in vitro* treatment of cancer cells with composite drug-loaded scaffolds and subsequent measurement of metabolic activity with AlamarBlue assay using a plate reader.

The high-resolution imaging of the 3D printed scaffolds was conducted with a Leica MS5 stereomicroscope, using the 4x objective magnification lens. A representative image of a scaffold can be found in Figure 1b.

Compression Testing

Five scaffolds with Lactoprene alone and nine composite scaffolds with Lactoprene and Lay FOMM 60 were printed and prepared prior to testing. The dimensions of the scaffolds were measured using a caliper. The average dimensions for the Lactoprene alone were 1.74 mm in height and 2.96 mm in diameter, and for Lactoprene with Lay FOMM 60, they were 1.86 mm in height and 3.03 mm in diameter. The cross-sectional area was calculated using the measurements to generate the stress-strain curves. The compression testing process can be found in Figure 2a.

In order to characterize the mechanical properties of the scaffolds, compression testing was performed using the Mini-Bionix 858 (MTS; 14000 Technology Dr. Eden Prairie, MN). All the scaffolds were tested with the same software: TestStar II (MTS: 14000 Technology Dr. Eden Prairie, MN). The maximum axial capacity was 10 kN, calibrated in the 2 kN range. The full scale was 2 kN and the hysteresis was set to 0.15% of full scale and the nonlinearity was 0.3% of full scale. The force and displacement data were recorded at 10 Hz. The strain rate was set to 1% strain/second. The compression test speed was set to 0.02 mm/second for a total deformation of 0.6 mm corresponding to 30% strain. The compression testing was programmed to start at 2.1 mm for clearance purposes and to compress to 1.4 mm. All compression tests were performed in a laboratory with ambient room temperature. The Young's moduli were calculated as the slopes of the linear portions of the stress-strain curves. The yield stresses were determined by a 0.02% offset method, and the yield strains were determined by the end of the linear portion of the stress-strain curves.

Cell lines and Chemotherapeutics

One of the cell lines used in this study was the triple-negative MDA-MB-231 breast cancer cell line expressing luciferase (MDA-MB-231/Luc), provided by the laboratory of Joan Massagué at Memorial Sloan Kettering Cancer Center. As well, MDA-MB231 cells expressing green fluorescent protein (GFP; MDA-MB-231/GFP) and IMR-90 mCherry fibroblasts (red fluorescent protein; RFP), both provided by the laboratory of professor M. Park at McGill University. The last cell line used in this study was the C4-2B (American Type Culture Collection; Manassas, VA, USA) prostate cancer cells. All cells were cultured in DMEM with the exception of C4-2B cells which were cultured in RPMI cell medium. Cells were cultured in complete cell medium containing 10% fetal bovine serum (FBS) and 1% penicillin-streptomycin. For *in vitro* assays, low-serum cell medium was used, which contained 1% FBS. The chemotherapeutics used were doxorubicin hydrochloride (Sigma-Aldrich) and cisplatin (Selleckchem).

Drug Release from Scaffolds

To evaluate the drug release profile of doxorubicin from the 3D printed scaffolds, three groups of scaffolds were prepared. Scaffolds were loaded with PBS (control) and 175 ng and 350 ng of doxorubicin. To load the drugs and PBS onto the scaffolds, the previously sterilized scaffolds were loaded with a 2 µL droplet of doxorubicin (150µM for 175ng and 300µM for 350ng) or PBS that was placed directly on top of the Lay FOMM core of the scaffold on one side. This was left to absorb into the LayFOMM core for 45 minutes. Additionally, 300 µL of PBS was placed in Eppendorf tubes. Once the scaffolds were dry, they were placed into the prepared tubes and stored in a 37°C incubator. The time points for drug release measurements were 5, 24, 48, 72, 120, and 168 hours. At these time points, half of the solution was removed without disturbing the scaffold and replaced with fresh PBS in all samples. The solution that was removed was used to measure

fluorescence intensity of doxorubicin using a TECAN Infinite M200 Pro microplate reader. The concentrations of doxorubicin were interpolated from a standard curve. The measurement of drug release overview can be found in Figure 2c.

Dose-Response

To assess drug efficacy against the MDA-MB-231/GFP and C4-2B cancer cell lines used in this study, dose-response assays were conducted. Briefly, 20,000 cells/well were plated in 48-well plates in fully-supplemented cell medium. The following day, cell medium was removed, and the cells were treated with 300 µL of various concentrations of doxorubicin or cisplatin in low-serum cell medium with PBS as a control. After 48h, the metabolic activity of cells was assessed via AlamarBlue (Invitrogen) resazurin reduction assays. The drug-containing medium was removed, and the wells received 100µL of a 10% AlamarBlue solution prepared in low-serum cell medium. The cells were incubated for 3h at 37ºC to allow for the reaction to occur. Following incubation, the fluorescence intensity of the metabolized AlamarBlue solution was measured with a TECAN Infinite M200 Pro microplate reader.

In Vitro Treatment

The response of MDA-MB-231/Luc and C4-2B cell lines to drug-loaded scaffolds was determined by the direct incubation of the scaffolds with the cells. Briefly, 20,000 cells were plated in 48 well plates. The following day, prepared scaffolds were incubated with the cells in low-serum cell medium. Four different experiments were conducted. Both cell lines were treated separately with doxorubicin and cisplatin. The concentration at which to load the two drugs on the two cancer cell lines was determined using the IC_{50} values obtained from the dose-response experiments. Doxorubicin-loaded scaffolds used with MDA-MB-231/Luc cells were loaded with 2 µL of 150

μM of doxorubicin. The direct positive control treatment of doxorubicin was 1 μM. Cisplatin scaffolds used with breast cancer cells were loaded with 2 μL of various concentrations of cisplatin (Table 1). The direct positive control treatment of cisplatin on breast cancer cells was 32 μM. Scaffolds loaded with doxorubicin for the treatment of C4-2B cells were loaded with 2 μL of 30 μM of doxorubicin. Direct positive control doxorubicin treatment in this experiment was loaded at 0.2 μM. Cisplatin scaffolds for the treatment of C4-2B cells were loaded with 2 μL of various concentrations of cisplatin (Table 2). The direct positive control cisplatin treatment was loaded at 8 μM. The cells were incubated with the scaffolds submerged in 500 μL of low-serum cell medium per well. After 5 days, the metabolic activity of cells was determined by AlamarBlue assays as described above. In Figure 2d, an overview of the *in vitro* treatment can be found.

Table 1. Scaffold cisplatin loading concentrations for in vitro MDA-MB-231/Luc cell treatment.

Scaffold	**Cisplatin Concentration Loaded (μM)**
A	2,667
B	5,333
C	8,000
D	10,666

Table 2. Scaffold cisplatin loading concentration for in vitro C4-2B cell treatment.

Scaffold	Cisplatin Concentration Loaded (μM)
E	1,200
F	1,867
G	2,667
H	5,333

3D In Vitro Treatment – Mixed Migration Model

To assess the migration of cells in a 3D model coupled with the 3D printed composite scaffolds as treatment (drug carrier), a mixed migration model (MMM) was conducted. A 3D interface model (PP-3D-S) comprised of a plasma-modified, electro-spun, nanofibrous 3D scaffold seeded with stromal cells as a stromal compartment and a 1% alginate-7% gelatin (A1G7) hydrogel mixture embedded with tumor cells as a tumor compartment was previously developed and used in this experiment to mimic a cancer microenvironment [21]. Briefly, to fabricate randomly oriented nanofibrous scaffolds with fiber diameters between about 600-800 nm, polylactic acid, PLA (NatureWorks 4032D, density = 1.24 g/cc) was electrospun, as previously shown [21], [22]. Treated electrospun scaffolds were cut into disks with a 9 mm punch and disinfected with RPMI medium containing 1% antibiotics and then placed into the wells of non-adherent 48-well polystyrene culture plates (SARSTEDT AG & Co.). Each well was seeded with 20,000 IMR-90 mCherry fibroblasts and incubated for 30 minutes in a humid atmosphere containing 5% carbon dioxide. After 30 min incubation, the liquid was removed from each well and mats were washed

with fresh media to remove non-adhering cells. Finally, a volume of 100 mL A1G7 hydrogel mixed with 50,000 tumor cell/well (MDA-MB 231/GFP) was applied on top of the pre-seeded nanofibrous scaffolds. Following this, 200 μL of 100 mM calcium dichloride, a crosslinking agent (calcium chloride dihydrate, C7902, Sigma), was added on top for ionic crosslinking. After 10 minutes, the residual crosslinking agent was removed and washed twice with fresh media, followed by adding 500 μL of media per well. This concludes the development of a compartmentalized 3D model, plasma-modified, electrospun 3D scaffold (PP-3D-S) combined with hydrogel. A more detailed description of the methodology is available in previous works [21], [22].

The summary of the MMM, which includes combining the 3D printed scaffolds with the PP-3D-S model, can be found in Figure 3. The same steps were followed for the direct treatment by using the PP-3D-S model without the 3D printed scaffold addition. The groups for this MMM consisted of a control, a 3D printed composite scaffold loaded with PBS, two differing doses of doxorubicin (500 μM, 600 μM) loaded onto 3D printed composite scaffolds and two direct positive control treatments with doxorubicin (1 μM, 2 μM). The doxorubicin doses to be loaded onto scaffolds were based on the IC_{50} data in this paper and the direct treatments were based on previously established IC_{50} values for the PP-3D-S model [21]. The 3D printed scaffolds were added directly on top of the PP-3D-S scaffolds. The experiment ran for 5 days before the AlamarBlue assay was performed to assess metabolic activity, as described previously. Before starting the assay, all 3D printed composite scaffolds loaded with drugs were removed and discarded.

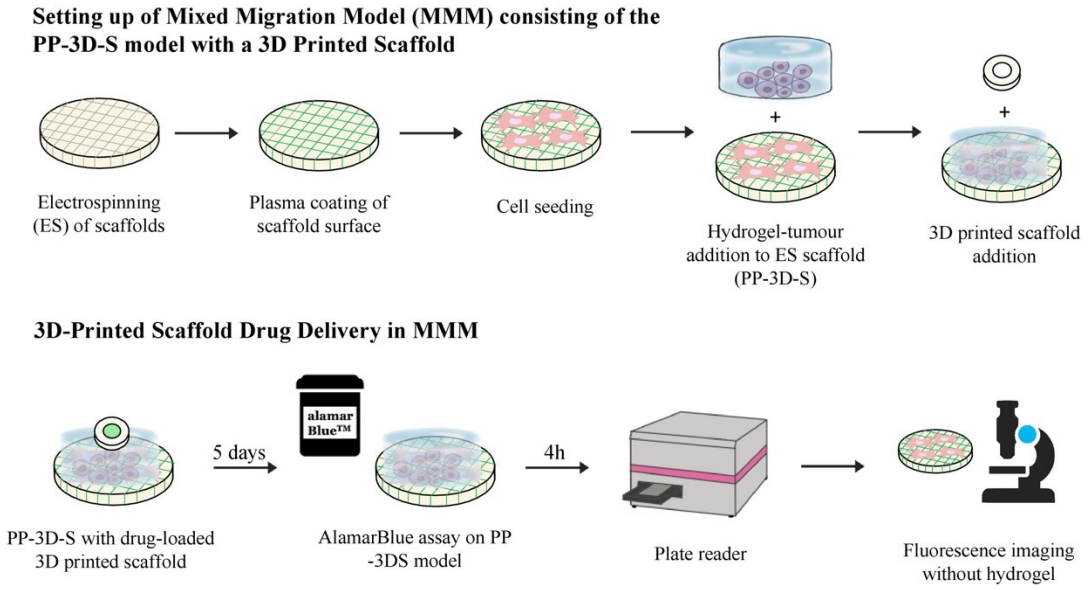

Figure 3. A schematic illustration of the MMM experiments, starting with the set-up of the MMM by combining PP-3D-S scaffolds with 3D printed scaffolds. Subsequent *in vitro* treatment of breast cancer cells using PP-3D-S scaffolds with 3D printed drug-infused scaffolds to test for metabolic activity and migration using a plate reader and fluorescence imaging, respectively.

The migration and invasion of breast cancer cells from hydrogel into the nanofibrous scaffolds (PP-3D-S model), was assessed using fluorescent imaging. After the AlamarBlue assay, the hydrogel was carefully scraped off the mat and the top surface of the scaffold was fixed with 4% paraformaldehyde (PFA) for 15 minutes at room temperature. Afterwards, the scaffolds were washed twice with PBS and placed on glass slides. To conduct imaging, an EVOS M5000 fluorescence microscope was used. A 4x-objective was used to capture images of the surface of the 9 mm mats. The tumor cells (GFP) appeared green and the fibroblasts (RFP) red in imaging. The number of migrated cells were counted using ImageJ software (National Institute of Health,

USA) and quantification was done in 20 different locations for each sample of three replicated experiments.

Statistical Analyses

Statistical tests were performed using GraphPad Prism 9.0 (GraphPad Software, La Jolla, CA, USA). Each experiment was performed thrice and in triplicate. The results are reported as mean ± SEM with an n = 3 unless otherwise indicated. Student's t tests were performed to test for significance between the mechanical properties of Lactoprene and composite scaffolds, as well as between the total amounts of doxorubicin released from scaffolds loaded with 175 and 350ng of doxorubicin. One-way ANOVAs were performed to test for significance between drug-loaded scaffold treatments. Dose-response data were fitted with sigmoidal functions and the IC_{50} values were determined by Prism. Statistical significance was taken as $p < 0.05$. The significance reported are the following: not significant (ns) $p > 0.05$; ** $p < 0.01$; **** $p < 0.0001$.

Results

Scaffold Fabrication and Compression Testing

The prepared composite Lay FOMM/Lactoprene scaffolds were approximately 2 mm in height and 3 mm in diameter. To assess the mechanical properties of the scaffolds, compression testing of both the outer Lactoprene shell (n = 5) as well as the composite scaffold (n = 9) was performed. Stress-strain curves were plotted (Figure 4a), and the mechanical properties were calculated. The Young's moduli of the Lactoprene shell and composite scaffolds were 198.96 MPa (±48.49 MPa) and 154.57 MPa (±58.86 MPa), respectively, however there were no statistically significant differences (Figure 4b, $p > 0.05$). The yield stress was 8.36 MPa (±0.88 MPa) for Lactoprene and 7.41 MPa (±2.85 MPa) for composite scaffolds. Similarly, there were no significant differences between the yield stresses (Figure 4c, $p > 0.05$). The composite scaffolds demonstrated an increase in the yield strain, which was calculated as a percent yield strain, from 5.56% (±0.94%) for Lactoprene scaffolds to 8.77% (±0.83%) for composite scaffolds, which was found to be a statistically significant difference in the amount of compression to reach the yield point (Figure 4d, $p < 0.0001$).

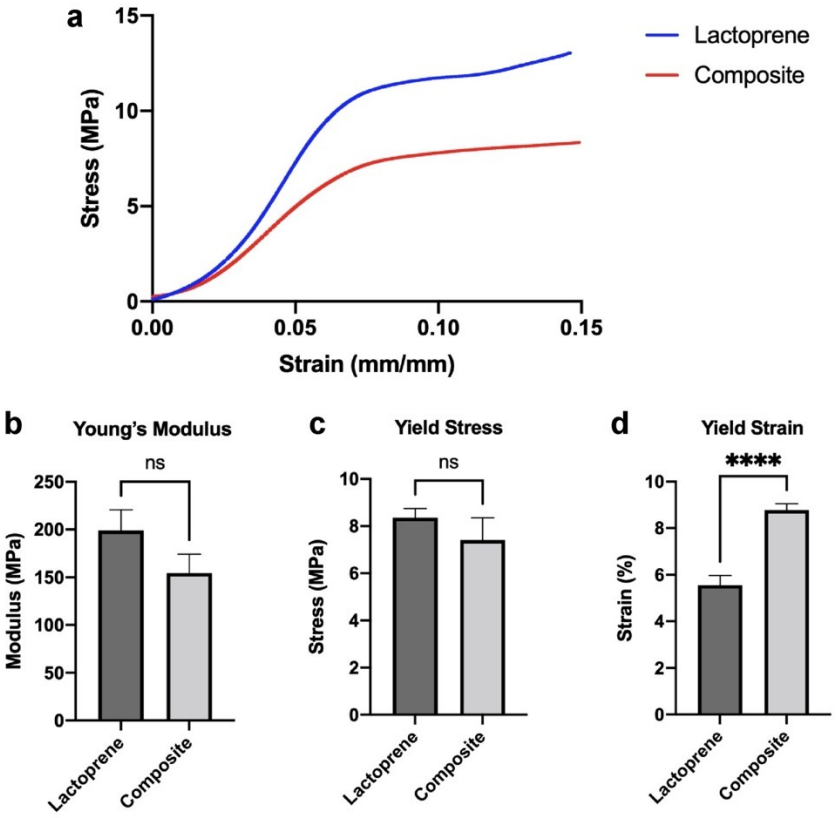

Figure 4. Compression testing was done on Lactoprene and composite scaffolds, yielding (a) stress-strain curves for Lactoprene (n = 5) and Composite scaffolds (n = 9). The three mechanical properties displayed are: (b) Young's modulus, (c) yield stress, and (d) yield strain.

Cumulative Doxorubicin Release from 3D Printed Scaffolds

We previously measured doxorubicin release from small scaffolds made of Lay FOMM 60 compared to other 3D printed scaffolds [20]. To determine the release kinetics when the Lay FOMM is part of a composite structure, we performed a similar release experiment. The release rate of doxorubicin from 3D printed composite scaffolds was quantified over a period of 7 days. The proportional release was not significantly different at the end of the 7-day period between scaffolds loaded with 175 ng and 350 ng of doxorubicin (Figure 5a, $p > 0.05$). The initial release of the scaffolds loaded with a higher amount of drug was higher, however, the difference became insignificant over the course of 7 days. Scaffolds loaded with 175 ng released 100.02 ng (±16.55 ng), which was 57.2% of the loaded amount, and those loaded with 350 ng released 226.53 ng (±19.98 ng), which was 64.7% of loaded amount, in 7 days (Figure 5b, $p < 0.0001$). Therefore, with more doxorubicin loaded, there is a significantly higher amount of doxorubicin released. However, the proportion of doxorubicin released did not significantly differ between the loading doses.

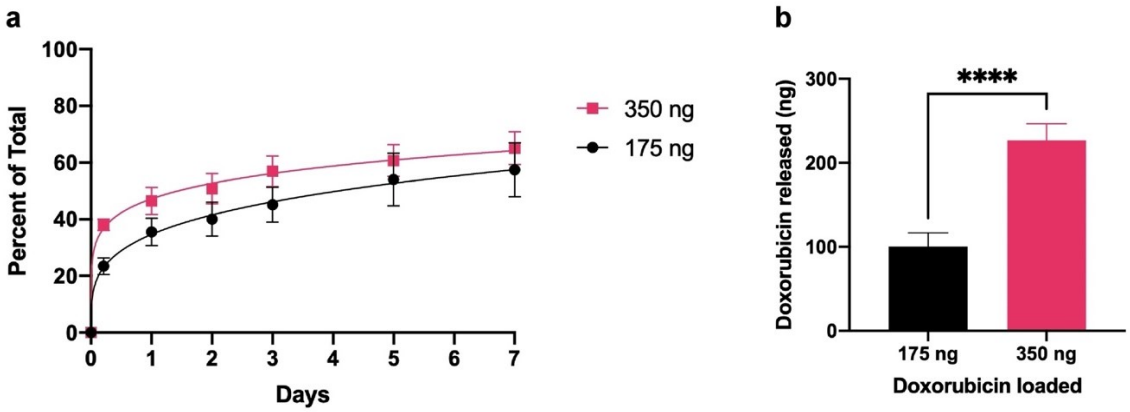

Figure 5. (a) Cumulative doxorubicin release from 3D printed composite scaffolds loaded with differing amounts (175, 350 ng) over the course of 7 days, expressed in percent of total drug loaded. (b) Amount of doxorubicin loaded as a function of doxorubicin released, expressed in nanograms. Data reported as mean ± SD with $n = 4$.

Dose-Response Curves

To determine the optimal drug loading concentrations for the 3D printed scaffolds, dose-response assays were conducted on MDA-MB-231/GFP and C4-2B cell lines. The MDA-MB-231/GFP cell line displayed a higher tolerance against both doxorubicin and cisplatin compared to the C4-2B line, with the relative IC_{50} values being 1.076 µM for doxorubicin and 34.21 µM for cisplatin (Figure 6a-b). The relative IC_{50} values for C4-2B cells for doxorubicin and cisplatin were determined to be 0.2651 µM and 7.933 µM, respectively (Figure 6c-d). Based on the drug release profile and IC_{50} values obtained, the 3D printed scaffolds were loaded with doxorubicin and cisplatin such that the released concentrations would fall in the therapeutic range. These loading concentrations are outlined in Table 1 and Table 2.

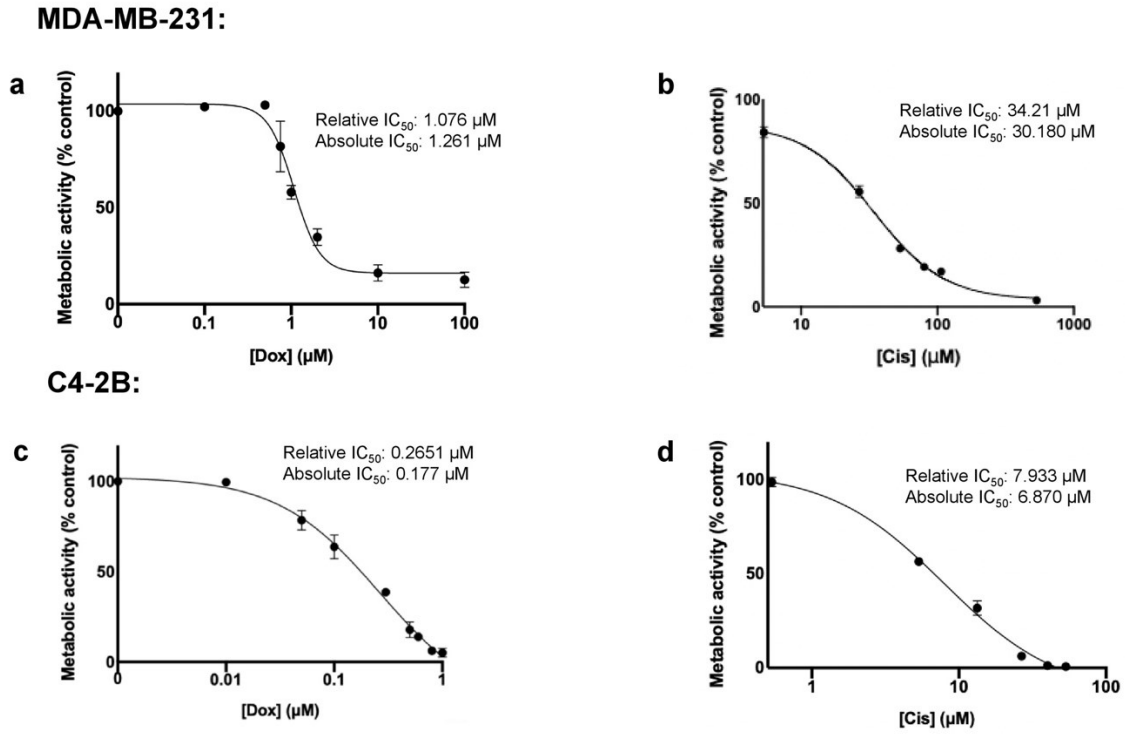

Figure 6. Relative IC_{50} curves determined for MDA-MB-231/GFP cells treated with chemotherapeutics (a) doxorubicin, and (b) cisplatin, as well as for C4-2B cells treated with (c) doxorubicin and (d) cisplatin.

3D Scaffold Drug Delivery to MDA-MB-231/Luc and C4-2B Cells

The drug-loaded scaffolds were incubated with the two cell lines to assess *in vitro* treatment efficacy. The doxorubicin release rate data was used to determine how much drug to load onto the scaffolds. For cisplatin, we used several cisplatin concentrations to create a standard curve in order to determine the optimal cisplatin release using AlamarBlue metabolic activity levels. MDA-MB-231/Luc cells treated with doxorubicin-infused composite scaffolds for 5 days showed a 87.64% (±2.52%) reduction in cell metabolic activity compared to cells treated with the control scaffolds loaded with PBS (Figure 7a, $p < 0.0001$). Similarly, all cisplatin-loaded scaffolds significantly

inhibited MDA-MB-231/Luc cell activity with a 63.77% (±2.57%) to 97.8% (±0.18%) reduction in activity depending on the loaded dose (Figure 7b, $p < 0.0001$). C4-2B cells treated with doxorubicin loaded scaffolds showed a 72.03% (±11.03%) reduction in metabolic activity compared to the control condition (Figure 7c, $p < 0.0001$). Likewise, all cisplatin-infused scaffolds significantly inhibited C4-2B cell activity by 72.82% (±3.82%) to 97.35% (±1.75%) (Figure 7d, $p < 0.0001$). Overall, higher loading doses of cisplatin provided a stronger effect with regards to cell metabolic activity inhibition. The metabolic activity of positive controls for both direct doxorubicin and cisplatin treatments were comparable to drug-infused scaffold treatments for both MDA-MB-231/Luc and C4-2B cell lines.

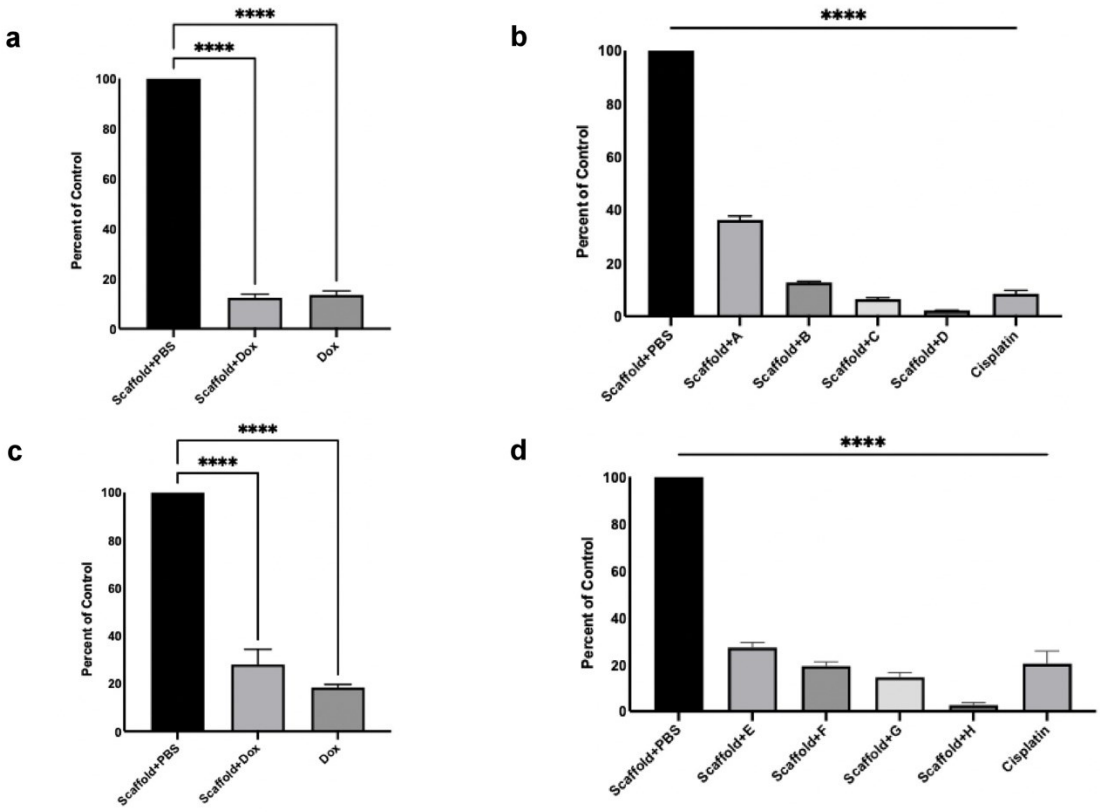

Figure 7. Metabolic activity of breast and prostate cancer cells measured with AlamarBlue assay after 5 days of treatment with 3D printed composite scaffolds loaded with PBS, doxorubicin(dox)

or cisplatin and direct drug treatment, expressed in percent of control. (a) MDA-MB-231/Luc cells with concentrations of 1 μM of free dox and 150 μM of dox-infused composite scaffolds; (b) MDA-MB-231/Luc cells with concentrations of 32 μM of free cisplatin and varying cisplatin doses loaded onto composite scaffolds; (c) C4-2B prostate cancer cell line with concentrations of 0.2 μM of free dox and 30 μM of dox-infused composite scaffolds; (d) C4-2B cells with concentrations of 8 μM of free cisplatin and varying cisplatin doses loaded onto composite scaffolds.

3D Scaffold Drug Delivery in Mixed Migration Model

To assess efficacy against cell activity and cell migration of the drug-loaded scaffolds in a physiologically-relevant 3D model, scaffolds were placed in our previously described PP-3D-S co-culture model with MDA-MB-231/GFP tumor cells and IMR-90 fibroblasts. When treated with doxorubicin-loaded scaffolds, fluorescence microscope images revealed a lower number of migrated tumor cells compared to direct doxorubicin treatment controls (Figure 8A). The reduction of cell metabolic activity with doxorubicin-loaded composite scaffolds and direct doxorubicin treatments (positive controls) was similar. The metabolic activity of the breast cancer cells was assessed in the PP-3D-S models with both drug-infused 3D printed composite scaffolds and direct treatments. The controls that were used as comparison for the 3D printed composite scaffolds were 3D printed scaffolds loaded with PBS, and for the direct treatment groups the controls were the PP-3D-S scaffolds in media with no treatment. Both 3D printed scaffolds and direct treatment significantly inhibited metabolic activity at all doses tested compared to their respective controls (Figure 8b, $p < 0.0001$). Finally, the number of migrated tumor cells were counted and demonstrated a 60.80% (±4.10%) to 66.69% (±1.42%) reduction in cell migration with doxorubicin-infused 3D printed composite scaffold treatment compared to controls (Figure 8c, $p < 0.01$).

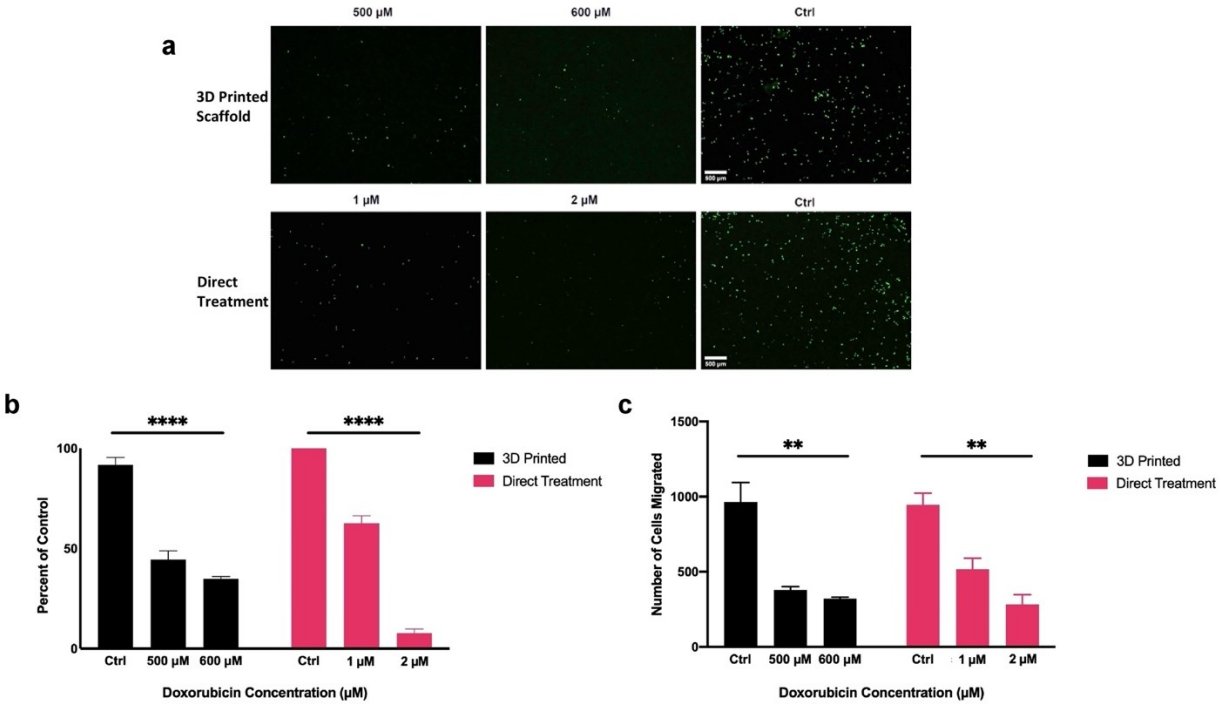

Figure 8. 3D printed composite scaffold drug delivery in Mixed Migration Model (MMM). (a) Fluorescence microscope images of migrated breast cancer cells with 3D printed scaffolds loaded with doxorubicin at 500 µM (n = 3) and 600 µM (n = 2), and direct treatment of 1 µM (n = 3) and 2 µM (n = 3) of doxorubicin. The controls were a scaffold loaded with PBS for the 3D printed condition and media with no drug for the direct treatment. (b) Metabolic activity of MDA-MB-231/GFP cells measured with AlamarBlue assay after 5 days of treatment with 3D printed and direct treatment at previously mentioned doses of doxorubicin compared to respective controls, expressed in percent of direct treatment control. (c) Number of migrated tumour cells counted with the same experimental and control groups and doses previously mentioned.

Discussion

The purpose of the study was to determine whether 3D printed composite scaffolds have comparable mechanical strength to trabecular bone and whether composite scaffolds loaded with chemotherapeutics will be equally effective at inhibiting tumor cell proliferation and migration *in vitro* compared to direct treatment. To assess this, compression testing of composite scaffolds, drug release measurement, IC_{50} determination, and 2D and 3D treatment with composite scaffolds were conducted.

Scaffold Fabrication and Compression Testing

The composite scaffolds were made from Lactoprene and Lay FOMM 60 materials, with the former used for 3D printing the shell and the latter consisting of the core that was fitted inside the shell. The composite scaffolds were subjected to compression testing to determine the mechanical properties, namely the Young's modulus, yield stress and the yield strain. In addition, stress-strain curves were generated. Young's modulus determines the stiffness of a material. There was no significant difference between the Lactoprene and composite scaffolds in terms of Young's modulus ($p > 0.05$). Given this, we can conclude that the addition of Lay FOMM in the composite scaffolds did not significantly lower the stiffness of the material, even though Lay FOMM is a more flexible material. The yield point is the limit of elastic behaviour and the start of plastic behaviour. The yield stress is the stress corresponding to the yield point, which is the force at which a material deforms and does not return to its original shape. There were no significant differences between Lactoprene and Lay FOMM in this parameter either, indicating that the addition of Lay FOMM does not significantly change the yield stress of the scaffolds ($p > 0.05$). The yield strain is the strain value corresponding to the yield stress. In this case, the percent strain at yield was significantly higher for the composite scaffolds compared to Lactoprene alone ($p <$

0.0001). This is because Lay FOMM is a porous, sponge-like material. The composite scaffolds can be compressed more due to their sponge-like property; therefore, the yield strain is a higher percentage of the strain given the original height, which was the height of the scaffold. These results indicate that the composite scaffolds have a more sponge-like property than the Lactoprene-only scaffolds, which may provide a cushioning effect in the bone to stabilize it without the addition of isolated pressure points.

There is an issue in heterogeneity in the mechanical properties of trabecular bone, namely due to variations in volume fraction, individual arrangement of trabeculae, aging and disease [23]. Due to this, there is a wide range found in the literature in terms of mechanical properties of trabecular bone. One study by Morgan and Keaveny (2001) determined the Young's modulus, yield stress and yield strain of vertebral trabecular bone with compression testing. They established the Young's modulus to be 344 MPa (±148) [24]. Other studies have found the Young's modulus for vertebral trabecular bone to be as low as 67 MPa (±45) [25]. In the current study, the value that was found for Young's modulus was 198.96 MPa (±48.49) for Lactoprene and 154.57 MPa (±58.86) for composite scaffolds. The Young's modulus of the Lactoprene and composite scaffolds in this study are within the range of what was found in the literature for vertebral trabecular bone. In one study, the yield stress was determined to be 2.02 MPa (±0.92), and the yield strain to be 0.77% (±0.06) [24]. The values for the yield stress and strain of Lactoprene and composite scaffolds in this study were determined to be higher than what has been found for vertebral trabecular bone. The stress is higher in the scaffolds at the limit of elastic behaviour compared to trabecular bone, which means that that they have the necessary capacity to bear weight.

Cumulative Doxorubicin Release from 3D Printed Scaffolds

The drug release kinetics of drug-loaded scaffolds were evaluated *in vitro* using a direct fluorescence method for doxorubicin and an indirect *in vitro* method using 2D cell culture for cisplatin. Composite scaffolds loaded with doxorubicin released approximately 60% of the loaded doxorubicin within a week, regardless of the amount loaded. The proportional release was nearly identical even with double the amount of loaded doxorubicin, indicating that the release is heavily dependent on the properties of the material used for drug delivery. Previous work in our group has indeed demonstrated that the drug release kinetics can be modified with the selection of different materials, with more porous materials leading to a higher proportional release over a period of one week [26]. As cisplatin is not fluorescent, various amounts were loaded onto scaffolds which were incubated with 2D cultures of MDA-MB-231 and C4-2B cells to determine drug release properties based on cell metabolic activity. Our results demonstrated that the release of cisplatin from the scaffolds was effective at inhibiting the cells *in vitro*, and that the effect was comparable to that of the direct cisplatin treatment. Therefore, the composite Lactoprene/Lay FOMM scaffolds were effective drug delivery devices *in vitro*. Dang *et al*. fabricated 3D printed scaffolds with micro- and macro-scale pores using PCL mixed with porogen microparticles [27]. They determined that the microscale porosity decreased the rapid initial release (burst release) of doxorubicin [27]. Multiple groups have 3D printed calcium phosphate cements for drug delivery application. Wu *et al*. explored calcium phosphate for the delivery of 5-fluorouracil, an anti-cancer drug, and the treated scaffolds released 100% of the loaded drug within 2 hours [28]. Drug release from calcium phosphate cement occurs rapidly in a burst release manner and is typically limited to a total release lasting less than 24 hours [29]. Zhu *et al*. combined mesoporous bioactive glasses and mesoporous silica nanoparticles with poly (3-hydroxybutyrate-co-3-hydroxyhexanoate) to generate composite

3D printed scaffolds [30]. They determined that with the addition of the mesoporous compounds, the release of anti-tuberculosis drugs was significantly prolonged compared to calcium phosphate cements [30]. Sustained released is more favorable in comparison to sustained release as it allows for long-term treatment and can suppress tumor growth at higher doses. In addition, burst release might be toxic for the adjacent healthy cells. In combination with our results, this demonstrates the importance of porous structures for 3D printed scaffolds intended for prolonged drug delivery applications and decreasing the burst release.

Dose Response & 3D Printed Scaffold Efficacy in 2D Culture

The dose response assays were conducted by treating MDA-MB-231 and C4-2B cancer cells with varying doses of doxorubicin and cisplatin for 48h, after which an AlamarBlue assay was used to assess the metabolic activity of the cells. These experiments were conducted to measure the potency of the drugs with reference to the specific cancer cell lines used in order to ascertain the appropriate amount of drug to load in subsequent experiments. The IC_{50} values were determined to be 1.076 μM and 34.21 μM for MDA-MB-231 cells treated with doxorubicin and cisplatin, respectively, and 0.2651 μM and 7.933 μM for C4-2B cells treated with doxorubicin and cisplatin, respectively. There is a disagreement in the IC_{50} values found in the literature due to a variety of factors, namely due to cell incubation time and type of assay used. Previous studies measured the IC_{50} values for MDA-MB-231 cells treated with doxorubicin and the values were between 1 and 3 μM [31]–[33]. This range is similar to the value found in this paper. As for MDA-MB-231 cells treated with cisplatin, the IC_{50} was determined to be in the range of 3 to 30 μM [34], [35]. One particular study used similar constraints but conducted a 48h MTT assay instead of a 48h AlamarBlue assay. They established the IC_{50} for MDA-MB-231 cells with cisplatin to be 23.0 μM [36]. The value determined in this paper of 34.21 μM falls close to the ranges found in the

literature. There is less research conducted on C4-2B cells, thus a comparison of IC_{50} data cannot be determined as these values were not found in the literature. Overall, the IC_{50} values determined in this paper were similar to what was found in the literature for MDA-MB-231 cells.

The 2D culture was developed by treating MDA-MB-231 and C4-2B cells with composite scaffolds loaded with chemotherapeutics doxorubicin and cisplatin separately. The cells were incubated and treated for 5 days and an AlamarBlue assay was conducted to assess metabolic activity. The metabolic activity for drug-infused composite scaffold treatments with both doxorubicin and cisplatin, separately, was significantly lower compared to negative controls (no treatment) and comparable to positive controls (direct chemotherapeutic treatments) for both MDA-MB-231/Luc and C4-2B cell lines. This demonstrates the composite scaffolds' ability to deliver chemotherapeutics *in vitro* and reduce the metabolic activity of cancer cells in a 2D culture. 2D culture *in vitro* models testing 3D printed scaffolds for treatment are currently being explored; however, the investigation in this study involves a novel material to elute drugs (Lay FOMM) that has a sustained release profile and is effective at inhibiting cancer cell metabolic activity. One study that used 3D printing for bone tissue engineering purposes involved encapsulating curcumin in liposomes to incorporate into a 3D printed calcium phosphate scaffold. The release of curcumin from the scaffolds was tested in a 2D model on both human fetal osteoblast cells and human osteosarcoma cells. The result was promotion of osteoblast cell viability, and cytotoxicity towards the osteosarcoma cells [37]. Another study set up an *in vitro* model with a 3D printed gelatin-based implant that could release chemotherapeutics and growth factors for osteogenesis and anti-tumor therapy. The metabolic activity of osteosarcoma-derived cell lines and breast cancer cells was assessed using a MTT assay. It was determined that the scaffolds loaded with cisplatin had lower cell viability compared to scaffolds without cisplatin, demonstrating their ability to release

chemotherapeutics and inhibit tumor growth [38]. There are studies investigating 3D printed scaffold uses in reducing metabolic activity of cancer cells *in vitro*, but their prevalence is still limited. Moreover, the fabrication process of the 3D printed scaffolds in the aforementioned studies are more time-consuming and complex as they involve an assembly process to derive the desired properties, such as porosity, whereas the 3D printed scaffolds proposed in this study have the desired properties embedded in the two filament types. As 2D models do not accurately recapitulate the target tumor microenvironment, there is a strong interest in 3D cell culture models for drug testing.

3D Scaffold Drug Delivery in Mixed Migration Model

To assess the migration of cancer cells in response to drug-loaded 3D printed scaffolds, a previously developed 3D co-culture migration model was used [21]. As 3D cell culture models are more realistic representations of cancer cell metastasis [39], this model allowed us to better evaluate the cellular response of doxorubicin eluted from the 3D composite scaffolds on cell metabolic activity and the number of cells that migrated onto the nanofibrous electrospun membrane. We determined that the effect of doxorubicin-loaded 3D printed scaffolds on MDA-MB-231 cells was comparable to the direct doxorubicin treatments with regards to both cell migration and metabolic activity after 5 days of treatment. There were very few cells that migrated to the electrospun membrane compared to the controls. The inhibition of metabolic activity and cell migration was dose-dependent, with higher doses leading to a stronger inhibitory effect. This demonstrates the ability of the scaffolds to impair cell activity and motility. To our knowledge, studies testing the effect of drug-loaded 3D printed scaffolds on cells in 3D culture models are limited. 2D culture models are typically used. Zhang *et al*. prepared composite PCL/hydrogel 3D printed scaffolds and loaded them with resveratrol and strontium ranelate to test their effect on the

migration of human umbilical vein endothelial cells using a standard wound healing assay [40]. They determined that scaffolds loaded with resveratrol showed the highest wound closure after 16h, however, the release could be carried out for 21 days with 30% of the loaded molecule released [40]. Wen *et al*. observed the migration of human mesenchymal stem cells (hMSCs) toward their water-based polyurethane 3D printed scaffolds loaded with chemokine SDF-1 and Y27632 [41]. Using a scratch assay to disrupt the 2D culture of hMSCs, they placed the scaffolds in a square wound created with a 1 mL pipette tip and determined that the loaded compounds increased cell migration towards the 3D printed scaffolds [41]. Studies assessing the efficacy of chemotherapeutic-loaded 3D printed scaffolds on cell migration are limited. Future studies evaluating cell motility are required to predict the success of these drug delivery devices and prevent pre-clinical failures with regards to the metastatic potential of the target tumors.

Limitations and Future Research

A key limitation of this research lies in the use of a proprietary material of which the precise composition is unknown. Furthermore, printing these materials requires optimization of the printing parameters which may not necessarily be identical for larger prints. The 3D printed scaffolds were loaded with doxorubicin and cisplatin on a single side, which may not have dispersed the drug solution homogeneously throughout the Lay FOMM core. It was assumed due to the drying that 100% of the drug was loaded onto the scaffold. The doxorubicin release kinetics were evaluated using a fluorescence microplate reader and interpolated from a standard curve, with samples taken at specified time points. Varying the volume of the aliquot taken and the volume replenished in the samples may affect the release rates of the drug, as the sink conditions would be affected. Future studies may assess drug release with varying sink conditions, as well as various release media other than PBS. Cisplatin release was measured indirectly by measuring cell

metabolic activity in response to the loaded scaffolds as the drug is not fluorescent. Subsequent studies may derivatize cisplatin with o-phenylenediamine to quantify it spectrophotometrically [42]. Furthermore, prolonging the experimental duration for measuring drug release kinetics would allow for a more complete release profile. The 2D and 3D *in vitro* cell metabolic activity and cell migration assays relied on the use of cell lines, which may not accurately depict tumor cells in their native tumor microenvironments. Although the 3D model is thought to be more representative, the use of patient-derived cells would strengthen the results and provide more information about the required drug doses as the dose-response curves may differ. Additionally, there is a possibility that the Lactoprene shell would not integrate with the bone in an *in vivo* model. It has not been established whether the chemotherapeutics would damage the surrounding healthy tissue, thereby prevent osseointegration. However, the chemotherapeutics specifically target rapidly dividing cells, making it less likely that osteoblasts and other bone cells would be targeted, and using a Lactoprene-β-TCP composite in an *in vivo* model could promote bony integration. Finally, the scaffolds' ability to attach cells and integrate into the target tissue, as well as the degradation rate of the scaffolds, may be evaluated to assess osseointegration and safety.

Conclusion

With the recent rise in cancer incidence and increased risk of recurrence and reoperation of metastatic bone lesions, the current surgical gold standard may be improved with 3D printed scaffolds for bone repair and drug delivery. We demonstrated here that 3D printed scaffolds can be manufactured at a low cost with mechanical properties similar to trabecular bone. Furthermore, the 3D printed composite scaffolds were loaded with doxorubicin and cisplatin chemotherapeutics and effective doses were released against breast and prostate cancer cells lines, inhibiting cell

activity and migration. An *in vivo* tumor metastasis model will allow for further pre-clinical testing of this drug delivery device to assess efficacy and ability to regenerate bone.

References

[1] T. N. Seyfried and L. C. Huysentruyt, "On the origin of cancer metastasis.," *Crit Rev Oncog*, vol. 18, no. 1–2, pp. 43–73, 2013, doi: 10.1615/critrevoncog.v18.i1-2.40.

[2] H. Soeharno, L. Povegliano, and P. F. Choong, "Multimodal treatment of bone metastasis - A surgical perspective," *Front Endocrinol (Lausanne)*, 2018, doi: 10.3389/fendo.2018.00518.

[3] N. Sundaresan, A. Rothman, K. Manhart, and K. Kelliher, "Surgery for solitary metastases of the spine: rationale and results of treatment. LK - https://mcgill.on.worldcat.org/oclc/112345142," *Spine TA - TT* -, vol. 27, no. 16, pp. 1802–1806, 2002.

[4] D. Shidid, M. Leary, P. Choong, and M. Brandt, "Just-in-time design and additive manufacture of patient-specific medical implants," *Phys Procedia*, vol. 83, pp. 4–14, 2016, doi: 10.1016/j.phpro.2016.08.002.

[5] P. Ahangar, M. E. Cooke, M. H. Weber, and D. H. Rosenzweig, "Current Biomedical Applications of 3D Printing and Additive Manufacturing," *Applied Sciences TA - TT* -, vol. 9, no. 8, p. 1713, 2019, doi: 10.3390/app9081713 LK - https://mcgill.on.worldcat.org/oclc/8163505422.

[6] X. Wang, M. Jiang, Z. Zhou, J. Gou, and D. Hui, "3D printing of polymer matrix composites: A review and prospective," *Composites Part B TA - TT* -, vol. 110, pp. 442–458, 2017, doi: 10.1016/j.compositesb.2016.11.034 LK - https://mcgill.on.worldcat.org/oclc/6953534614.

[7] A. A. Pitaru *et al.*, "Investigating Commercial Filaments for 3D Printing of Stiff and Elastic Constructs with Ligament-Like Mechanics," *Micromachines TA - TT* -, vol. 11, no. 9, p. 846, 2020, doi: 10.3390/mi11090846 LK - https://mcgill.on.worldcat.org/oclc/8661893870.

[8] R. Fairag *et al.*, “A Composite Lactide-Mineral 3D-Printed Scaffold for Bone Repair and Regeneration.,” *Frontiers in cell and developmental biology TA - TT -*, vol. 9, p. 654518, 2021, doi: 10.3389/fcell.2021.654518 LK - https://mcgill.on.worldcat.org/oclc/9135314817.

[9] M. Aquib *et al.*, “Advances in local and systemic drug delivery systems for post-surgical cancer treatment.,” *Journal of materials chemistry. B TA - TT -*, vol. 8, no. 37, pp. 8507–8518, 2020, doi: 10.1039/d0tb00987c LK - https://mcgill.on.worldcat.org/oclc/8653421003.

[10] E. P. Goldberg, A. R. Hadba, B. A. Almond, and J. S. Marotta, “Intratumoral cancer chemotherapy and immunotherapy: opportunities for nonsystemic preoperative drug delivery,” *Journal of Pharmacy and Pharmacology TA - TT -*, vol. 54, no. 2, pp. 159–180, 2010, doi: 10.1211/0022357021778268 LK - https://mcgill.on.worldcat.org/oclc/4650295076.

[11] G. Chindamo, S. Sapino, E. Peira, D. Chirio, M. C. Gonzalez, and M. Gallarate, “Bone Diseases: Current Approach and Future Perspectives in Drug Delivery Systems for Bone Targeted Therapeutics.,” *Nanomaterials (Basel, Switzerland) TA - TT -*, vol. 10, no. 5, 2020, doi: 10.3390/nano10050875 LK - https://mcgill.on.worldcat.org/oclc/8587796272.

[12] E. L. Cyphert, N. Kanagasegar, N. Zhang, G. D. Learn, and H. A. von Recum, “PMMA Bone Cement Composite Functions as an Adjuvant Chemotherapeutic Platform for Localized and Multi-Window Release during Bone Reconstruction,” *Macromolecular Bioscience TA - TT -*, vol. 22, no. 5, 2022, doi: 10.1002/mabi.202100415 LK - https://mcgill.on.worldcat.org/oclc/9501297168.

[13] H.-J. Jiang *et al.*, “Mechanical Properties and Cytocompatibility Improvement of Vertebroplasty PMMA Bone Cements by Incorporating Mineralized Collagen,” *Materials*, vol. 5. pp. 2616–2634, 2015. doi: 10.3390/ma8052616 LK - https://mcgill.on.worldcat.org/oclc/8773563792.

[14] M. Arora, E. K. S. Chan, S. Gupta, and A. D. Diwan, “Polymethylmethacrylate bone cements and additives: A review of the literature,” *World Journal of Orthopedics TA - TT -*, vol. 4, no. 2, pp. 67–74, 2013, doi: 10.5312/wjo.v4.i2.67 LK - https://mcgill.on.worldcat.org/oclc/8145676102.

[15] M. A. Lopez-Heredia, G. J. B. Kamphuis, P. C. Thüne, F. C. Oner, J. A. Jansen, and X. F. Walboomers, “An injectable calcium phosphate cement for the local delivery of paclitaxel to bone LK - https://mcgill.on.worldcat.org/oclc/8087189521,” *Biomaterials TA - TT -*, vol. 32, no. 23, pp. 5411–5416, 2011.

[16] R. Krüger, J.-M. Seitz, A. Ewald, F.-W. Bach, and J. Groll, “Strong and tough magnesium wire reinforced phosphate cement composites for load-bearing bone replacement,” *Journal of the Mechanical Behavior of Biomedical Materials TA - TT -*, vol. 20, pp. 36–44, 2013, doi: 10.1016/j.jmbbm.2012.12.012 LK - https://mcgill.on.worldcat.org/oclc/4948360024.

[17] W. Dang *et al.*, “Hemin particles-functionalized 3D printed scaffolds for combined photothermal and chemotherapy of osteosarcoma,” *Chemical Engineering Journal TA - TT -*, vol. 422, 2021, doi: 10.1016/j.cej.2021.129919 LK - https://mcgill.on.worldcat.org/oclc/9007767060.

[18] P. J. Kondiah, P. P. D. Kondiah, Y. E. Choonara, T. Marimuthu, and V. Pillay, “A 3D Bioprinted Pseudo-Bone Drug Delivery Scaffold for Bone Tissue Engineering.,” *Pharmaceutics TA - TT -*, vol. 12, no. 2, 2020, doi: 10.3390/pharmaceutics12020166 LK - https://mcgill.on.worldcat.org/oclc/8536245925.

[19] H. Wang *et al.*, “A novel vehicle-like drug delivery 3D printing scaffold and its applications for a rat femoral bone repairing in vitro and in vivo.,” *International journal of biological sciences*

TA - TT -, vol. 16, no. 11, pp. 1821–1832, 2020, doi: 10.7150/ijbs.37552 LK - https://mcgill.on.worldcat.org/oclc/8591939899.

[20] P. Ahangar, E. Akoury, A. S. R. G. Luna, A. Nour, M. H. Weber, and D. H. Rosenzweig, "Nanoporous 3D-printed scaffolds for local doxorubicin delivery in bone metastases secondary to prostate cancer," *Materials*, vol. 11, no. 9, 2018, doi: 10.3390/ma11091485.

[21] M. Mohseni Garakani *et al.*, "A novel 3D co-culture platform for integrating tissue interfaces for tumor growth, migration and therapeutic sensitivity: 'PP-3D-S,'" *Biomaterials Advances TA - TT* -, vol. 134, 2022, doi: 10.1016/j.msec.2021.112566 LK - https://mcgill.on.worldcat.org/oclc/9346321637.

[22] M. Mohseni Garakani, M. E. Cooke, M. R. Wertheimer, D. H. Rosenzweig, and A. Ajji, "A novel 3D in vitro tissue model for bone-metastasized breast cancer: A preclinical tool in drug discovery and testing," *Plasma Processes and Polymers TA - TT* -, vol. 19, no. 7, 2022, doi: 10.1002/ppap.202100206 LK - https://mcgill.on.worldcat.org/oclc/9548593976.

[23] T. M. Keaveny, E. F. Morgan, G. L. Niebur, and O. C. Yeh, "Biomechanics of Trabecular Bone," *Annual Review of Biomedical Engineering TA - TT* -, vol. 3, no. 1, pp. 307–333, 2001, doi: 10.1146/annurev.bioeng.3.1.307 LK - https://mcgill.on.worldcat.org/oclc/4656828591.

[24] E. F. Morgan and T. M. Keaveny, "Dependence of yield strain of human trabecular bone on anatomic site," *Journal of Biomechanics TA - TT* -, vol. 34, no. 5, pp. 569–577, 2001, doi: 10.1016/S0021-9290(01)00011-2 LK - https://mcgill.on.worldcat.org/oclc/4923948260.

[25] Li. Mosekilde, Le. Mosekilde, and C. C. Danielsen, "Biomechanical competence of vertebral trabecular bone in relation to ash density and age in normal individuals," *Bone TA - TT* -, vol. 8,

no. 2, pp. 79–85, 1987, doi: 10.1016/8756-3282(87)90074-3 LK - https://mcgill.on.worldcat.org/oclc/4934624704.

[26] P. Ahangar, E. Akoury, A. S. Ramirez Garcia Luna, A. Nour, M. H. Weber, and D. H. Rosenzweig, "Nanoporous 3D-Printed Scaffolds for Local Doxorubicin Delivery in Bone Metastases Secondary to Prostate Cancer," *Materials TA - TT* -, vol. 11, no. 9, 2018, doi: 10.3390/ma11091485 LK - https://mcgill.on.worldcat.org/oclc/8147882719.

[27] H. P. Dang *et al.*, "3D printed dual macro-, microscale porous network as a tissue engineering scaffold with drug delivering function," *TA - TT* -, vol. 11, no. 3, 2019, doi: 10.1088/1758-5090/ab14ff LK - https://mcgill.on.worldcat.org/oclc/8083133524.

[28] Y. Wu, L. Woodbine, A. M. Carr, A. R. Pillai, A. Nokhodchi, and M. Maniruzzaman, "3D Printed Calcium Phosphate Cement (CPC) Scaffolds for Anti-Cancer Drug Delivery.," *Pharmaceutics TA - TT* -, vol. 12, no. 11, 2020, doi: 10.3390/pharmaceutics12111077 LK - https://mcgill.on.worldcat.org/oclc/8695514578.

[29] R. Trombetta, J. A. Inzana, E. M. Schwarz, S. L. Kates, and H. A. Awad, "3D Printing of Calcium Phosphate Ceramics for Bone Tissue Engineering and Drug Delivery," *Annals of biomedical engineering TA - TT* -, vol. 45, no. 1, pp. 23–44, 2017, doi: 10.1007/s10439-016-1678-3 LK - https://mcgill.on.worldcat.org/oclc/8148160183.

[30] M. Z., Y. Z., J. Z., K. L., and X. Y., "3D-printed hierarchical scaffold for localized isoniazid/rifampin drug delivery and osteoarticular tuberculosis therapy," *Acta Biomaterialia TA - TT* -, vol. 16, no. 1, pp. 145–155, 2015, doi: 10.1016/j.actbio.2015.01.034 LK - https://mcgill.on.worldcat.org/oclc/8088337637.

[31] A. Mishra, S. K. Mukhopadhyay, and S. Dey, “Evaluation of Cyclosaplin Efficacy Using a Silk Based 3D Tumor Model,” *Biomolecules TA - TT -*, vol. 9, no. 4, 2019, doi: 10.3390/biom9040123 LK - https://mcgill.on.worldcat.org/oclc/8291662440.

[32] S. Wen, S. Su, B. Liou, C. Lin, and K. Lee, “Sulbactam-enhanced cytotoxicity of doxorubicin in breast cancer cells,” *Cancer Cell International*, vol. 18. pp. 1–18, 2018. doi: 10.1186/s12935-018-0625-9 LK - https://mcgill.on.worldcat.org/oclc/7828095283.

[33] N. Pilco-Ferreto and G. M. Calaf, “Influence of doxorubicin on apoptosis and oxidative stress in breast cancer cell lines.,” *International journal of oncology TA - TT -*, vol. 49, no. 2, pp. 753–762, 2016, doi: 10.3892/ijo.2016.3558 LK - https://mcgill.on.worldcat.org/oclc/6218132744.

[34] F. Lucantoni, A. U. Lindner, N. O’Donovan, H. Düssmann, and J. H. M. Prehn, “Systems modeling accurately predicts responses to genotoxic agents and their synergism with BCL-2 inhibitors in triple negative breast cancer cells.,” *Cell death & disease TA - TT -*, vol. 9, no. 2, p. 42, 2018, doi: 10.1038/s41419-017-0039-y LK - https://mcgill.on.worldcat.org/oclc/7342569162.

[35] A. Wawruszak *et al.*, “Assessment of Interactions between Cisplatin and Two Histone Deacetylase Inhibitors in MCF7, T47D and MDA-MB-231 Human Breast Cancer Cell Lines - An Isobolographic Analysis.,” *PloS one TA - TT -*, vol. 10, no. 11, p. e0143013, 2015, doi: 10.1371/journal.pone.0143013 LK - https://mcgill.on.worldcat.org/oclc/5923210224.

[36] A. Z. M. Pauzi *et al.*, “Combination of cisplatin and bromelain exerts synergistic cytotoxic effects against breast cancer cell line MDA-MB-231 in vitro,” *Chinese Medicine*, vol. 11. pp. 1–11, 2016. doi: 10.1186/s13020-016-0118-5 LK - https://mcgill.on.worldcat.org/oclc/9523130788.

[37] N. Sarkar and S. Bose, “Liposome-Encapsulated Curcumin-Loaded 3D Printed Scaffold for Bone Tissue Engineering.,” *ACS applied materials & interfaces TA - TT* -, vol. 11, no. 19, pp. 17184–17192, 2019, doi: 10.1021/acsami.9b01218 LK - https://mcgill.on.worldcat.org/oclc/8036608518.

[38] Y. Jiang *et al.*, “Bioinspired adhesive and tumor microenvironment responsive nanoMOFs assembled 3D-printed scaffold for anti-tumor therapy and bone regeneration,” *Nano Today TA - TT* -, vol. 39, 2021, doi: 10.1016/j.nantod.2021.101182 LK - https://mcgill.on.worldcat.org/oclc/9040666916.

[39] K. Duval *et al.*, “Modeling Physiological Events in 2D vs. 3D Cell Culture LK - https://mcgill.on.worldcat.org/oclc/7095978565,” *Physiology. TA - TT* -, vol. 32, no. 1000028, pp. 266–277, 2017.

[40] W. Zhang *et al.*, “3D printed composite scaffolds with dual small molecule delivery for mandibular bone regeneration,” *TA - TT* -, vol. 12, no. 3, 2020, doi: 10.1088/1758-5090/ab906e LK - https://mcgill.on.worldcat.org/oclc/8608914468.

[41] Y.-T. Wen, N.-T. Dai, and S.-H. Hsu, “Biodegradable water-based polyurethane scaffolds with a sequential release function for cell-free cartilage tissue engineering.,” *Acta biomaterialia TA - TT* -, vol. 88, pp. 301–313, 2019, doi: 10.1016/j.actbio.2019.02.044 LK - https://mcgill.on.worldcat.org/oclc/8014559465.

[42] B. Anilanmert, G. Yalcin, F. Arioz, and E. Dolen, “THE SPECTROPHOTOMETRIC DETERMINATION OF CISPLATIN IN URINE, USING o-PHENYLENEDIAMINE AS DERIVATIZING AGENT LK - https://mcgill.on.worldcat.org/oclc/618614275,” *Analytical Letters TA - TT* -, vol. 34, no. 1, pp. 113–123, 2001.

Chapter IV: Conclusion

In this thesis, we developed a composite scaffold using Lactoprene and Lay FOMM 60 with the aim of providing mechanical stability and locally delivering chemotherapeutics in a bone metastases environment. We tested the mechanical properties of the composite scaffolds through compression testing and determined that the 3D printed scaffolds have similar mechanical properties to trabecular bone, whereby the Young's modulus of the composite scaffolds was 154.57 MPa (± 58.86), which is in the range of what is found in the literature for vertebral trabecular bone. The drug release profile from the composite scaffolds was evaluated and dose response assays were conducted to test the drug efficacy against the breast and prostate cancer cell lines. A 2D and 3D cell culture model was set up to determine the effect of the composite scaffolds loaded with chemotherapeutics on metabolic activity and migration of cancer cells. More specifically, in a 2D culture, the composite scaffolds loaded with doxorubicin and cisplatin, separately, were able to significantly reduce the metabolic activity of both the breast and prostate cancer cell lines compared to controls ($p < 0.0001$). In the 3D model previously described, doxorubicin-loaded composite scaffolds significantly inhibited metabolic activity of the MDA-MB-231 cells at all tested doses compared to controls ($p < 0.0001$) and significantly reduced tumor cell migration compared to controls ($p < 0.01$). Overall, the mechanically stable 3D printed composite scaffolds can release chemotherapeutics, are useful for locally reducing proliferation of metastatic bone cancers and have good potential for bone repair. To our knowledge, research looking into the use of drug-loaded 3D printed scaffolds as devices for the treatment of bone cancer, specifically in locally delivering chemotherapeutics and providing mechanical stability to a bone defect, is limited. The use of Lay FOMM as a drug-eluting core in a 3D printed scaffold is

especially sparse in the literature. This research has the potential to lead to improved surgical outcomes in spine oncology patients. Locally delivering anti-cancer drugs avoids side effects and complications typically seen with systemic chemotherapy. There is also the potential for advancement of treatment in cancer therapy, improvement of bone metastases prognosis in patients and their overall quality of life, and reduction of cost and burden of patients in the healthcare system.

References

[1] H. Soeharno, L. Povegliano, and P. F. Choong, "Multimodal treatment of bone metastasis - A surgical perspective," *Front Endocrinol (Lausanne)*, 2018, doi: 10.3389/fendo.2018.00518.

[2] S. Mercadante, "Malignant bone pain: pathophysiology and treatment," *Pain TA - TT* -, vol. 69, no. 1, pp. 1–18, 1997, doi: 10.1016/S0304-3959(96)03267-8 LK - https://mcgill.on.worldcat.org/oclc/4930970956.

[3] G. Guzik, "Oncological and functional results after surgical treatment of bone metastases at the proximal femur," *BMC Surg*, vol. 18, no. 1, pp. 2–9, 2018, doi: 10.1186/s12893-018-0336-0.

[4] B. M. Liu, M. Li, B. S. Yin, J. Y. Zou, W. G. Zhang, and S. Y. Wang, "Effects of incorporating carboxymethyl chitosan into PMMA bone cement containing methotrexate," *PLoS One*, vol. 10, no. 12, pp. 1–20, 2015, doi: 10.1371/journal.pone.0144407.

[5] W. R. Moore, S. E. Graves, and G. I. Bain, "Synthetic bone graft substitutes," *ANZ J Surg*, vol. 71, no. 6, pp. 354–361, 2001, doi: 10.1046/j.1440-1622.2001.02128.x.

[6] D. Shidid, M. Leary, P. Choong, and M. Brandt, "Just-in-time design and additive manufacture of patient-specific medical implants," *Phys Procedia*, vol. 83, pp. 4–14, 2016, doi: 10.1016/j.phpro.2016.08.002.

[7] A. Nooh *et al.*, “Intra-tumor delivery of zoledronate mitigates metastasis-induced osteolysis superior to systemic administration,” *J Bone Oncol*, vol. 6, no. October 2016, pp. 8–15, 2017, doi: 10.1016/j.jbo.2017.01.001.

[8] G. Maccauro, M. S. Spinelli, S. Mauro, C. Perisano, C. Graci, and M. A. Rosa, “Physiopathology of Spine Metastasis,” *International Journal of Surgical Oncology*, vol. 2011. 2011. doi: 10.1155/2011/107969 LK - https://mcgill.on.worldcat.org/oclc/8090969933.

[9] R. G. Perrin and A. W. Laxton, “Metastatic spine disease: epidemiology, pathophysiology, and evaluation of patients. LK - https://mcgill.on.worldcat.org/oclc/110418084,” *Neurosurgery clinics of North America TA - TT* -, vol. 15, no. 4, pp. 365–373, 2004.

[10] R. Harel and L. Angelov, “Spine metastases: Current treatments and future directions,” *European Journal of Cancer TA - TT* -, vol. 46, no. 15, pp. 2696–2707, 2010, doi: 10.1016/j.ejca.2010.04.025 LK - https://mcgill.on.worldcat.org/oclc/4930652080.

[11] P. Ahangar, M. Aziz, D. H. Rosenzweig, and M. H. Weber, “Advances in personalized treatment of metastatic spine disease,” *Annals of Translational Medicine TA - TT* -, vol. 7, no. 10, p. 223, 2019, doi: 10.21037/atm.2019.04.41 LK - https://mcgill.on.worldcat.org/oclc/8175823499.

[12] D. M. Sciubba and Z. L. Gokaslan, “Diagnosis and management of metastatic spine disease,” *Surgical Oncology TA - TT* -, vol. 15, no. 3, pp. 141–151, 2006, doi: 10.1016/j.suronc.2006.11.002 LK - https://mcgill.on.worldcat.org/oclc/4931035167.

[13] U. Schick, G. Marquardt, and R. Lorenz, “Intradural and extradural spinal metastases,” *Neurosurgical Review TA - TT* -, vol. 24, no. 1, pp. 1–5, 2001, doi: 10.1007/PL00011959 LK - https://mcgill.on.worldcat.org/oclc/5649228766.

[14] W. B. Jacobs and R. G. Perrin, “Evaluation and treatment of spinal metastases: an overview,” *Neurosurgical Focus TA - TT* -, vol. 11, no. 6, pp. 1–11, 2001, doi: 10.3171/foc.2001.11.6.11 LK - https://mcgill.on.worldcat.org/oclc/4665621335.

[15] W. A. Sifuentes Giraldo, V. Pachón Olmos, J. I. Gallego Rivera, and M. Vázquez Díaz, “Multiple vertebral metastases with fluid-fluid levels.,” *Reumatologia clinica TA - TT* -, vol. 10, no. 5, pp. 338–339, 2014, doi: 10.1016/j.reuma.2013.10.003 LK - https://mcgill.on.worldcat.org/oclc/5644322515.

[16] K.-S. Delank, C. Wendtner, H. T. Eich, and P. Eysel, “The treatment of spinal metastases.,” *Deutsches Arzteblatt international TA - TT* -, vol. 108, no. 5, pp. 71–79, 2011, doi: 10.3238/arztebl.2011.0071 LK - https://mcgill.on.worldcat.org/oclc/704671423.

[17] L. M. Shah and K. L. Salzman, “Imaging of spinal metastatic disease.,” *Int J Surg Oncol*, vol. 2011, p. 769753, 2011, doi: 10.1155/2011/769753.

[18] I. Laufer *et al.*, “The NOMS framework: approach to the treatment of spinal metastatic tumors.,” *Oncologist*, vol. 18, no. 6, pp. 744–751, Jun. 2013, doi: 10.1634/theoncologist.2012-0293.

[19] A. D. Bhatt, J. C. Schuler, M. Boakye, and S. Y. Woo, “Current and emerging concepts in non-invasive and minimally invasive management of spine metastasis.,” *Cancer Treat Rev*, vol. 39, no. 2, pp. 142–152, Apr. 2013, doi: 10.1016/j.ctrv.2012.08.002.

[20] M. Mossa-Basha *et al.*, “Spinal metastasis: diagnosis, management and follow-up.,” *Br J Radiol*, vol. 92, no. 1103, p. 20190211, Nov. 2019, doi: 10.1259/bjr.20190211.

[21] M. Aquib *et al.*, “Advances in local and systemic drug delivery systems for post-surgical cancer treatment.,” *Journal of materials chemistry. B TA - TT -*, vol. 8, no. 37, pp. 8507–8518, 2020, doi: 10.1039/d0tb00987c LK - https://mcgill.on.worldcat.org/oclc/8653421003.

[22] V. Kurisunkal, A. Gulia, and S. Gupta, “Principles of Management of Spine Metastasis.,” *Indian J Orthop*, vol. 54, no. 2, pp. 181–193, Apr. 2020, doi: 10.1007/s43465-019-00008-2.

[23] S. Ryu, H. Yoon, A. Stessin, F. Gutman, A. Rosiello, and R. Davis, “Contemporary treatment with radiosurgery for spine metastasis and spinal cord compression in 2015.,” *Radiation oncology journal TA - TT -*, vol. 33, no. 1, pp. 1–11, 2015, doi: 10.3857/roj.2015.33.1.1 LK - https://mcgill.on.worldcat.org/oclc/5810856658.

[24] M. J. Provenzano, K. P. J. Murphy, and L. H. 3rd Riley, “Bone cements: review of their physiochemical and biochemical properties in percutaneous vertebroplasty.,” *AJNR Am J Neuroradiol*, vol. 25, no. 7, pp. 1286–1290, Aug. 2004.

[25] C. M. Sayama, M. H. Schmidt, and E. F. Bisson, “Cervical spine metastases: techniques for anterior reconstruction and stabilization.,” *Neurosurgical review TA - TT -*, vol. 35, no. 4, pp. 463–474, 2012, doi: 10.1007/s10143-012-0388-z LK - https://mcgill.on.worldcat.org/oclc/810001685.

[26] O. Diegel, “Additive Manufacturing: An Overview,” in *Comprehensive Materials Processing*, Elsevier Ltd, 2014, pp. 3–18. doi: 10.1016/B978-0-08-096532-1.01000-1 LK - https://mcgill.on.worldcat.org/oclc/5594870366.

[27] B. P. Chan and K. W. Leong, “Scaffolding in tissue engineering: general approaches and tissue-specific considerations,” *European Spine Journal TA - TT -*, vol. 17, no. S4, pp. 467–479, 2008, doi: 10.1007/s00586-008-0745-3 LK - https://mcgill.on.worldcat.org/oclc/4959749780.

[28] A. Gleadall, D. Visscher, J. Yang, D. Thomas, and J. Segal, “Review of additive manufactured tissue engineering scaffolds: relationship between geometry and performance,” *Burns & Trauma*, vol. 6. p. 19, 2018. doi: 10.1186/s41038-018-0121-4 LK - https://mcgill.on.worldcat.org/oclc/8254956207.

[29] P. Ahangar, M. E. Cooke, M. H. Weber, and D. H. Rosenzweig, “Current Biomedical Applications of 3D Printing and Additive Manufacturing,” *Applied Sciences TA - TT -*, vol. 9, no. 8, p. 1713, 2019, doi: 10.3390/app9081713 LK - https://mcgill.on.worldcat.org/oclc/8163505422.

[30] A. S. Alagoz and V. Hasirci, “3D printing of polymeric tissue engineering scaffolds using open-source fused deposition modeling,” *Emergent Materials*, vol. 3. pp. 429–439, 2020. doi: 10.1007/s42247-019-00048-2 LK - https://mcgill.on.worldcat.org/oclc/8657938372.

[31] X. Wang, M. Jiang, Z. Zhou, J. Gou, and D. Hui, “3D printing of polymer matrix composites: A review and prospective,” *Composites Part B TA - TT -*, vol. 110, pp. 442–458, 2017, doi: 10.1016/j.compositesb.2016.11.034 LK - https://mcgill.on.worldcat.org/oclc/6953534614.

[32] P. Ahangar, E. Akoury, A. S. Ramirez Garcia Luna, A. Nour, M. H. Weber, and D. H. Rosenzweig, “Nanoporous 3D-Printed Scaffolds for Local Doxorubicin Delivery in Bone Metastases Secondary to Prostate Cancer,” *Materials TA - TT* -, vol. 11, no. 9, 2018, doi: 10.3390/ma11091485 LK - https://mcgill.on.worldcat.org/oclc/8147882719.

[33] E. Tosoratti, P. Fisch, S. Taylor, L. A. Laurent-Applegate, and M. Zenobi-Wong, “3D-Printed Reinforcement Scaffolds with Targeted Biodegradation Properties for the Tissue Engineering of Articular Cartilage,” *Advanced Healthcare Materials TA - TT* -, vol. 10, no. 23, 2021, doi: 10.1002/adhm.202101094 LK - https://mcgill.on.worldcat.org/oclc/9354010164.

[34] R. Fairag *et al.*, “A Composite Lactide-Mineral 3D-Printed Scaffold for Bone Repair and Regeneration.,” *Frontiers in cell and developmental biology TA - TT* -, vol. 9, p. 654518, 2021, doi: 10.3389/fcell.2021.654518 LK - https://mcgill.on.worldcat.org/oclc/9135314817.

[35] R. Cailleau, M. Olivé, and Q. V. J. Cruciger, “Long-Term Human Breast Carcinoma Cell Lines of Metastatic Origin: Preliminary Characterization LK - https://mcgill.on.worldcat.org/oclc/5550948863,” *In Vitro TA - TT* -, vol. 14, no. 11, pp. 911–915, 1978.

[36] H. Liu, C. Zang, M. H. Fenner, K. Possinger, and E. Elstner, “PPARgamma ligands and ATRA inhibit the invasion of human breast cancer cells in vitro. LK - https://mcgill.on.worldcat.org/oclc/110981067,” *Breast cancer research and treatment TA - TT* -, vol. 79, no. 1, pp. 63–74, 2003.

[37] K. J. Chavez, S. V. Garimella, and S. Lipkowitz, “Triple negative breast cancer cell lines: One tool in the search for better treatment of triple negative breast cancer,” *Breast Disease TA - TT* -, vol. 32, no. 1–2, pp. 35–48, 2010, doi: 10.3233/BD-2010-0307 LK - https://mcgill.on.worldcat.org/oclc/761894556.

[38] L. Spans *et al.*, “Comparative genomic and transcriptomic analyses of LNCaP and C4-2B prostate cancer cell lines.,” *PloS one TA - TT* -, vol. 9, no. 2, p. e90002, 2014, doi: 10.1371/journal.pone.0090002 LK - https://mcgill.on.worldcat.org/oclc/5539592660.

[39] M. Shields, “Chapter 14 - Chemotherapeutics,” S. Badal and R. B. T.-P. Delgoda, Eds. Boston: Academic Press, 2017, pp. 295–313. doi: https://doi.org/10.1016/B978-0-12-802104-0.00014-7.

[40] The American Cancer Society medical and editorial content team, “Chemotherapy for Bone Cancer,” *The American Cancer Society*, 2021. https://www.cancer.org/cancer/bone-cancer/treating/chemotherapy.html

[41] K. Johnson-Arbor and R. Dubey, “Doxorubicin.,” Treasure Island (FL), 2022.

[42] S. Shah *et al.*, “Fluorescence properties of doxorubicin in PBS buffer and PVA films.,” *J Photochem Photobiol B*, vol. 170, pp. 65–69, May 2017, doi: 10.1016/j.jphotobiol.2017.03.024.

[43] J. M. Gold and A. Raja, “Cisplatin.,” Treasure Island (FL), 2022.

[44] A. Brown, S. Kumar, and P. B. Tchounwou, “Cisplatin-Based Chemotherapy of Human Cancers.,” *J Cancer Sci Ther*, vol. 11, no. 4, 2019.

[45] S. Dasari and P. B. Tchounwou, “Cisplatin in cancer therapy: molecular mechanisms of action.,” *Eur J Pharmacol*, vol. 740, pp. 364–378, Oct. 2014, doi: 10.1016/j.ejphar.2014.07.025.

[46] K. Maharajan, “Feasibility of local administration of chemotherapeutic drugs as an effective adjuvant therapy in primary, recurrent and metastatic extradural tumours of the spine-review.,” *J Spine Surg*, vol. 5, no. 2, pp. 273–284, Jun. 2019, doi: 10.21037/jss.2019.04.11.

[47] E. P. Goldberg, A. R. Hadba, B. A. Almond, and J. S. Marotta, “Intratumoral cancer chemotherapy and immunotherapy: opportunities for nonsystemic preoperative drug delivery,” *Journal of Pharmacy and Pharmacology TA - TT -*, vol. 54, no. 2, pp. 159–180, 2010, doi: 10.1211/0022357021778268 LK - https://mcgill.on.worldcat.org/oclc/4650295076.

[48] X. Ma *et al.*, “Titanium Implants and Local Drug Delivery Systems Become Mutual Promoters in Orthopedic Clinics,” vol. 12. p. 47, 2021. doi: 10.3390/nano12010047 LK - https://mcgill.on.worldcat.org/oclc/9456287382.

[49] G. Chindamo, S. Sapino, E. Peira, D. Chirio, M. C. Gonzalez, and M. Gallarate, “Bone Diseases: Current Approach and Future Perspectives in Drug Delivery Systems for Bone Targeted Therapeutics.,” *Nanomaterials (Basel, Switzerland) TA - TT -*, vol. 10, no. 5, 2020, doi: 10.3390/nano10050875 LK - https://mcgill.on.worldcat.org/oclc/8587796272.

[50] M. Chen *et al.*, “Construction of multilayered molecular reservoirs on a titanium alloy implant for combinational drug delivery to promote osseointegration in osteoporotic

conditions," *Acta Biomaterialia TA - TT* -, vol. 105, pp. 304–318, 2020, doi: 10.1016/j.actbio.2020.01.029 LK - https://mcgill.on.worldcat.org/oclc/8544106633.

[51] K. Gulati, M. S. Aw, and D. Losic, "Drug-eluting Ti wires with titania nanotube arrays for bone fixation and reduced bone infection," *Nanoscale Research Letters TA - TT* -, vol. 6, no. 1, pp. 1–6, 2011, doi: 10.1186/1556-276X-6-571 LK - https://mcgill.on.worldcat.org/oclc/5660122383.

[52] A.-M. le Ray *et al.*, "Vancomycin encapsulation in biodegradable poly(ε-caprolactone) microparticles for bone implantation. Influence of the formulation process on size, drug loading, in vitro release and cytocompatibility," *Biomaterials TA - TT* -, vol. 24, no. 3, pp. 443–449, 2003, doi: 10.1016/S0142-9612(02)00357-5 LK - https://mcgill.on.worldcat.org/oclc/4929073747.

[53] S. Bose, N. Sarkar, and D. Banerjee, "Effects of PCL, PEG and PLGA polymers on curcumin release from calcium phosphate matrix for **in vitro** and **in vivo** bone regeneration," *TA - TT* -, vol. 8, pp. 110–120, 2018, doi: 10.1016/j.mtchem.2018.03.005 LK - https://mcgill.on.worldcat.org/oclc/8017124703.

[54] Y. Wu, L. Woodbine, A. M. Carr, A. R. Pillai, A. Nokhodchi, and M. Maniruzzaman, "3D Printed Calcium Phosphate Cement (CPC) Scaffolds for Anti-Cancer Drug Delivery.," *Pharmaceutics TA - TT* -, vol. 12, no. 11, 2020, doi: 10.3390/pharmaceutics12111077 LK - https://mcgill.on.worldcat.org/oclc/8695514578.

[55] J. Zhang *et al.*, "3D-printed magnetic Fe3O4/MBG/PCL composite scaffolds with multifunctionality of bone regeneration, local anticancer drug delivery and hyperthermia,"

Journal of Materials Chemistry B TA - TT -, vol. 2, no. 43, pp. 7583–7595, 2014, doi: 10.1039/c4tb01063a LK - https://mcgill.on.worldcat.org/oclc/5686824032.

[56] Y. Wang *et al.*, "3D printed biodegradable implants as an individualized drug delivery system for local chemotherapy of osteosarcoma," *TA - TT* -, vol. 186, 2020, doi: 10.1016/j.matdes.2019.108336 LK - https://mcgill.on.worldcat.org/oclc/8507334372.

[57] E. L. Cyphert, N. Kanagasegar, N. Zhang, G. D. Learn, and H. A. von Recum, "PMMA Bone Cement Composite Functions as an Adjuvant Chemotherapeutic Platform for Localized and Multi-Window Release during Bone Reconstruction," *Macromolecular Bioscience TA - TT* -, vol. 22, no. 5, 2022, doi: 10.1002/mabi.202100415 LK - https://mcgill.on.worldcat.org/oclc/9501297168.

[58] H.-J. Jiang *et al.*, "Mechanical Properties and Cytocompatibility Improvement of Vertebroplasty PMMA Bone Cements by Incorporating Mineralized Collagen," *Materials*, vol. 5. pp. 2616–2634, 2015. doi: 10.3390/ma8052616 LK - https://mcgill.on.worldcat.org/oclc/8773563792.

[59] M. Arora, E. K. S. Chan, S. Gupta, and A. D. Diwan, "Polymethylmethacrylate bone cements and additives: A review of the literature," *World Journal of Orthopedics TA - TT* -, vol. 4, no. 2, pp. 67–74, 2013, doi: 10.5312/wjo.v4.i2.67 LK - https://mcgill.on.worldcat.org/oclc/8145676102.

[60] M. A. Lopez-Heredia, G. J. B. Kamphuis, P. C. Thüne, F. C. Oner, J. A. Jansen, and X. F. Walboomers, "An injectable calcium phosphate cement for the local delivery of paclitaxel to bone LK - https://mcgill.on.worldcat.org/oclc/8087189521," *Biomaterials TA - TT* -, vol. 32, no. 23, pp. 5411–5416, 2011.

[61] R. Krüger, J.-M. Seitz, A. Ewald, F.-W. Bach, and J. Groll, “Strong and tough magnesium wire reinforced phosphate cement composites for load-bearing bone replacement,” *Journal of the Mechanical Behavior of Biomedical Materials TA - TT -*, vol. 20, pp. 36–44, 2013, doi: 10.1016/j.jmbbm.2012.12.012 LK - https://mcgill.on.worldcat.org/oclc/4948360024.

[62] P. J. Kondiah, P. P. D. Kondiah, Y. E. Choonara, T. Marimuthu, and V. Pillay, “A 3D Bioprinted Pseudo-Bone Drug Delivery Scaffold for Bone Tissue Engineering.,” *Pharmaceutics TA - TT -*, vol. 12, no. 2, 2020, doi: 10.3390/pharmaceutics12020166 LK - https://mcgill.on.worldcat.org/oclc/8536245925.

[63] H. Wang *et al.*, “A novel vehicle-like drug delivery 3D printing scaffold and its applications for a rat femoral bone repairing in vitro and in vivo.,” *International journal of biological sciences TA - TT -*, vol. 16, no. 11, pp. 1821–1832, 2020, doi: 10.7150/ijbs.37552 LK - https://mcgill.on.worldcat.org/oclc/8591939899.

[64] W. Dang *et al.*, “Hemin particles-functionalized 3D printed scaffolds for combined photothermal and chemotherapy of osteosarcoma,” *Chemical Engineering Journal TA - TT -*, vol. 422, 2021, doi: 10.1016/j.cej.2021.129919 LK - https://mcgill.on.worldcat.org/oclc/9007767060.